# Pairing of Single Electron Additions at the Edge of an Ultraclean Mini 2DEG

by

Ahmet Demir

B.S., Electrical & Electronics Engineering (2011)
B.S., Physics (2011)
Bogazici University

Submitted to the Department of Physics
in partial fulfillment of the requirements for the degree of

Doctor of Philosophy in Physics

at the

MASSACHUSETTS INSTITUTE OF TECHNOLOGY

February 2019



Author .....
Department of Physics
January 11, 2019

Certified by .....
Raymond C. Ashoori
Professor of Physics
Thesis Supervisor

Accepted by .....
Nergis Mavalvala
Associate Department Head, Physics

# Pairing of Single Electron Additions at the Edge of an Ultraclean Mini 2DEG

by

Ahmet Demir

Submitted to the Department of Physics
on January 11, 2019, in partial fulfillment of the
requirements for the degree of
Doctor of Philosophy in Physics

## Abstract

In this work, we created laterally large and low disorder quantum well based quantum dots to study single electron additions to two dimensional electron gas systems(2DEG). Their single electron addition spectra has been studied using a capacitance technique in a dilution refrigerator. As a function of magnetic field and density, we measured the single electron addition energies from a completely empty dot, up to dot occupancies of thousands of electrons. For small dots, at low density and magnetic field, we found the expected non-interacting Fock-Darwin behavior. However, at high density and high magnetic field, we observed deviations from single particle picture which is suggestive of more novel physics.

To observe collective behaviour in quantum dots, we created relatively larger quantum dots so that the dot would behave as a small two dimensional(2D) system. However, observing such behavior has been challenging due to the difficulty in the fabrication of sufficiently high quality devices. The quantum dots we are working on differ from those of previous works in that they do not contain any modulation doping nor a Schottky barrier above the dot. This new design eliminates all unscreened dopants. Instead, we populate carriers electrostatically by an external gate.

Here, we report the observation in the addition spectra of interaction driven localized states and isolated tunneling to edge states. We see electron additions to the edge states between filling factors $\nu = 1$ and $\nu = 2$ with single flux quantum (h/e) periodicity in magnetic field. Remarkably, between filling factors $\nu = 2$ and $\nu = 5$, we observe the pairing of electron additions to states at the edges of the quantum dots with a corresponding 2e charge tunneling. Near filling factor 5/2 and at fixed gate voltage, these twice-height peaks appear uniformly with a periodicity of h/2e. At other filling factors in the range $\nu = 2 - 5$, the mean periodicity for the twice-height electron peaks remains h/2e, but the twice-height peaks are instead further bunched into pairs, with pairs spaced h/e apart. The filling factors for the observed h/2e periodicity coincide with those of a pairing phenomenon seen in conductance oscillations in Fabry-Perot interferometers[1] that indicated inter-channel entanglement between edge channels. Moreover, the unusual 2-electron Coulomb blockade peaks suggest a

pair tunneling effect that involves electron correlations that arise in the quantum dot.

Thesis Supervisor: Raymond C. Ashoori
Title: Professor of Physics

*to my parents*

# Acknowledgments

Throughout my PhD years, I am grateful for spending most of my twenties in an amazing place fulfilling my childhood dreams. It has been a very awarding seven years and truly thorough experience to have become a part of this community at MIT.

I would like to first thank my advisor, Prof. Ray Ashoori, who took me as a graduate student and gave his utmost guidance during the entire program. I consider myself very fortunate to have the opportunity to learn many aspects of condensed matter experiment from one of the defining scholars in the field. Ray exemplifies how physical intuition and simple understanding works. Keeping up with his standards in publishing a work, giving a talk, and just explaining the simple physical concepts has been very rewarding. I would also like to express my deep gratitude to Pablo Jarillo-Herrero and Leonid Levitov for becoming my thesis committee.

I would also like to thank my post-doc, effectively my second advisor, Neal Staley. Not only was his guidance and his expertise in condensed matter physics invaluable at the early stage of my life in MIT, he also helped me in many ways throughout my graduate career. With him, I learned how to systematically approach my career goals, and achieving them in small steps. I thank him for his patience in answering our countless questions.

MIT offers me a unique intellectual environment where I can meet a lot of talented and passionate physicists. I would like to thank Spencer Tomarken, my colleague and office mate. Over so many years, we collaborated on many projects and shared insights every day. In the last couple years, we also started working out and gained a physical strength that I never had before. We defined ourselves as the "linear boys" for always having straight gains in our strength.

I would like to also thank to some of other members of the Ashoori lab for being around for all those years. Joonho Jang, Andrea Young, Heun Mo Yoo, Ben Hunt were some of the people I have learned a lot during the first years of the program and I continued receiving their feedback about the experiments and the physics. I am

also grateful for many fellow graduate students around me, who made my life at MIT stimulating both academically and socially. Of course, I would like to thank Physics Department's administrator staff for being always available and supportive. Thank you Monica Wolf, Sydney Miller, and Catherine Modica!

I am also thankful for all of my friends in Camberville area. Among them my best friend Melih Okan has a special place for which we shared similar struggles for so many years and supported each other. During one of the most difficult experiences of our lives, the PhD program, we strived from each other's friendship. Him and other so many friends, including Erman and Selcuk, made a lot of my weekends and holidays memorable moments of my graduate life.

Finally, I want to thank my family for their understanding and support in me choosing the career of physics abroad.

The work at MIT was funded by the Basic Energy Sciences Program of the Office of Science of the U.S. Department of Energy through contract no. FG02-08ER46514.

THIS PAGE INTENTIONALLY LEFT BLANK

# Contents

# List of Figures

# List of Tables

THIS PAGE INTENTIONALLY LEFT BLANK

# Chapter 1

# Introduction

This thesis is comprised of three parts. The first part consists of an introduction into two dimensional electron gas(2DEG) physics and the single electron capacitance spectroscopy(SECS). In Chapter 2, we describe the experimental techniques ranging from the the fabrication of a quantum dots to low temperature amplifiers and the capacitance bridge. Going through numerous variations and iterations in the fabrication process and measurement scheme, we were able to detect single electron additions to a small dot. The second part(Chapter 3) of this thesis deals with small dots in which we mostly observe single particle physics. These dots display Coulomb blockade physics, Fock-Darwin spectrum and some deviations from the single particle physics that is driven by interactions between electrons. In the third part(Chapter 4 and 5), we explore the crossover regime to a mini 2DEG. This part contains a number of new results, not present in the literature, and not expected when we started this project. We see electron additions to the edge states between filling factors $\nu = 1$ and $\nu = 2$ with single flux quantum (h/e) periodicity in magnetic field. Moreover, between filling factors $\nu = 2$ and $\nu = 5$, we observe the pairing of electron additions to states at the edges of the quantum dots with a corresponding 2e charge tunneling.

## 1.1 Two Dimensional Electron Gas Systems

With the discovery of the integer quantum Hall effect in 1980[2], a new domain in physics has opened, and it still remains to be an active area of research. Classically, the electrical Hall conductance is expected to have a linear relation between the applied magnetic field and the measured Hall conductance. What has been observed in 1980 was, instead, the quantization of the conductance at certain values. The Hall conductance versus the magnetic field manifests itself as a staircase(Fig 1-1) with quantized conductance given by an integer times the fundamental unit of conductance, $e^2/h$. High precision experiments showed that this value is extremely accurate and is independent of the sample.

In just less than two years after the discovery of integer quantum Hall effect in 1982, fractional quantum Hall effect was realized[3]. This time, the quantized value took on fractional values of fundamental unit of conductance. The integer effect is caused by the strong magnetic field and the presence of the impurities which tend to enhance the stability of plateau. To observe the fractional effect, the samples must be extremely clean. It turns out, the mechanism behind fractional effect is electron-electron interaction whereas integer effect is a single particle effect[4, 5, 6].

The quenching of kinetic energy of electrons in Landau levels under strong magnetic field enables a number of intriguing phases developed due to dominant electron-electron correlation. With advanced fabrication skills, we now can create structures with unparalleled cleanliness and quality. Although there is a rich pool of studies of both theoretical and experimental understanding of the quantum Hall system in semiconductors, there is active study and debate about the energy scales[8, 9], the transport mechanisms[10, 11], and the nature of the ground state[12, 13] for many quantum Hall features.

We study on high quality 2DEGs created in GaAs/AlGaAs heterostructures grown by molecular beam epitaxy (MBE). This new crystal growth technique was first used by groups in Bell labs[14] to increase the mobility of charge carriers. In MBE, a semiconductor crystal can be grown a single atomic layer at a time. By varying the

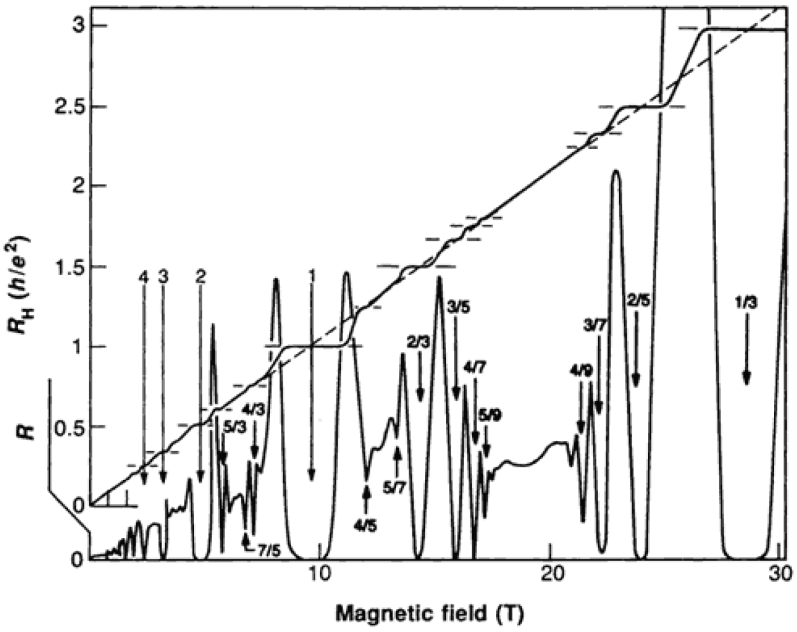


Figure 1-1: Transport measurements showing plateau at Hall resistance for integer and fractional quantum Hall states[7].

chemical composition, epitaxial layers consistent of different semiconductor materials can be grown on top of each other. Furthermore, by selecting lattice matched semiconductors, this can be done in a way that produces a nearly perfect crystal with few defects. For a 23nm GaAs quantum well, the confinement energy difference between the first band and the second band is about $\frac{h^2}{2m_e^* L^2} = 47\,\text{meV}$ where , $m_e^*$=0.063 $m_e$ is the band mass of electrons in GaAs. The Fermi energy is only $\epsilon_F = n\frac{\pi\hbar^2}{m_e^*} = 3.8\,\text{meV}$ at a typical 2D electron density of $n = 10^{11} cm^{-2}$. Since the measurement temperature is well below 1K(0.1 meV), we can safely assume electrons lie in the first band, and thermal activation to second subband is nonexistent.

Confining a 2DEG laterally, one can confine particles in three dimensions producing a quantum dot(QD). As in an atom, the energy levels in a quantum dot become quantized due to the confinement of electrons. The main advantage of artificial atoms in experiment is that you can tune their size, shape and electron occupancy. In that sense it provides a simple system to study confined electrons and their interactions in

response to an external parameter such as magnetic field or confinement potential.

Conventionally quantum dots have been studied extensively using transport measurements on lateral quantum dots[15, 16], with the exception of transport studies in vertical structures[17, 18]. Lateral transport measurements of QD structures are challenging for many reasons: using lateral plunger gates gives different gating for different states and the lateral systems only couple to states at the edge. In order to access the single electron addition spectrum of laterally large quantum-confined structures, we have developed a vertical tunneling geometry which avoids these pitfalls associated with lateral contacts and allows us to track electron additions up to thousands of electrons over a wide range of magnetic field. Studying electron additions to vertical quantum dots provides the capability for sensing both localized and extended states of electrons[19, 20, 21, 22].

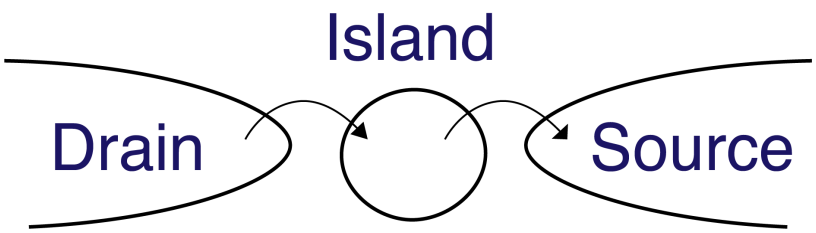


Figure 1-2: Tunneling of electrons between drain and source through an intermediate island.

## 1.2 Coulomb Blockade

When we add/subtract electrons to a metal island or a quantum dot, there are different energy scales that we need to consider. Therefore, it is essential to comprehend how Coulomb blockade works. To begin with, consider a charge transport experiment in which charge flows from drain to source through an intermediate metal island as in Fig 1-2. We assume conduction of electrons through insulating gaps occurs by quantum tunneling. When a tunneling event happens from drain to the metal island, the charge on the island is suddenly increases by the quantized amount e. If the electrostatic energy $e^2/C_\Sigma$ of single excess electron on the island($C_\Sigma$ is the total capacitance of the island to the rest of the world) is much greater than electron thermal energy $k_BT$, the second electron cannot be transferred from reservoir to the island. This is simply because there isn't any electron with sufficiently high energy in the reservoir to tunnel into the island that already has one electron. This suppression is called Coulomb blockade[23, 24].

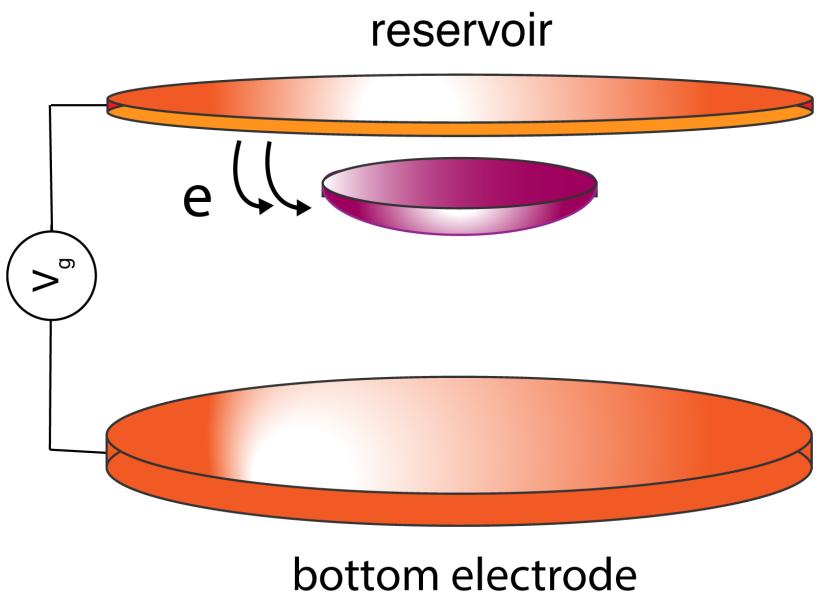


Figure 1-3: A small metallic island is coupled to a reservoir and a gate electrode. Electron transfer can occur only between the island and the reservoir through a tunneling barrier. Gate electrode is coupled capacitively and is used to adjust the electrostatic potential of the island.

In the capacitance measurements we use a system that is depicted in the Figure 1-3. A small metallic island coupled to an infinite reservoir of electrons and a gate. Particle exchange can occur only by tunneling through a barrier between the island and the reservoir. The gate is coupled to the island only electrostatically, and can be used to attract or repel particles into the island. When a tunneling event happens from the reservoir to the island, it increases the Coulomb energy of the island by $e^2/C_\Sigma$. If this charging energy is much higher than $k_BT$, then the second electron cannot be transfered to the island. We can write the first condition as,

$$k_BT \ll e^2/C_\Sigma \tag{1.1}$$

Secondly, we want the number of electrons on the island to be well quantized. This means that the uncertainty in an electron's energy $\Delta E$ due to electron's time spending on the island, $\Delta t$, must be smaller than the charging energy. This condition

requires the barrier between the island and the reservoir to be opaque enough so that the electrons are localized in the reservoir or on the island.

$$\Delta E \approx h/\Delta t \ll e^2/C_\Sigma \tag{1.2}$$

This implies that both tunneling resistance should have a lower bound[25, 26],

$$R_t \gg h/e^2 \tag{1.3}$$

The first condition can be met by making the dot smaller and cooling the entire system to low temperatures. The second one can be met by weakly coupling of the island to the reservoir.

THIS PAGE INTENTIONALLY LEFT BLANK

# Chapter 2

# Single Electron Capacitance Measurements

Throughout this thesis, our goal is to find an unknown capacitance as a function of gate voltage or magnetic field. We use single electron capacitance spectroscopy(SECS) which has been developed in Ashoori Lab[22, 27], and then we improved this technique over the years, increased the sensitivity substantially.

## 2.1 MBE Wafer

We have developed a platform to create quantum well based large QDs with very low disorder. The dot is confined between two electrodes in the "tunnel capacitor" structure shown in Fig 2-1. This dot differs from those of previous works in Ref [28] in that it does not contain any modulation doping nor a Schottky barrier above the dot. Instead, we have developed a new sample design that incorporates a small ohmic contact on top of a etched pillar. This new design eliminates all unscreened dopants. Instead, we populate the QD with electrons entirely by gating.

To investigate fractional quantum Hall states in the single electron resolution level, we need ultraclean devices and significantly improved signal to noise ratio. To create the cleanest structure we have worked with Dr. Loren Pfeiffer at Princeton to create an "inverted" tunneling structure utilizing cold growth GaAs diffusion barriers. In

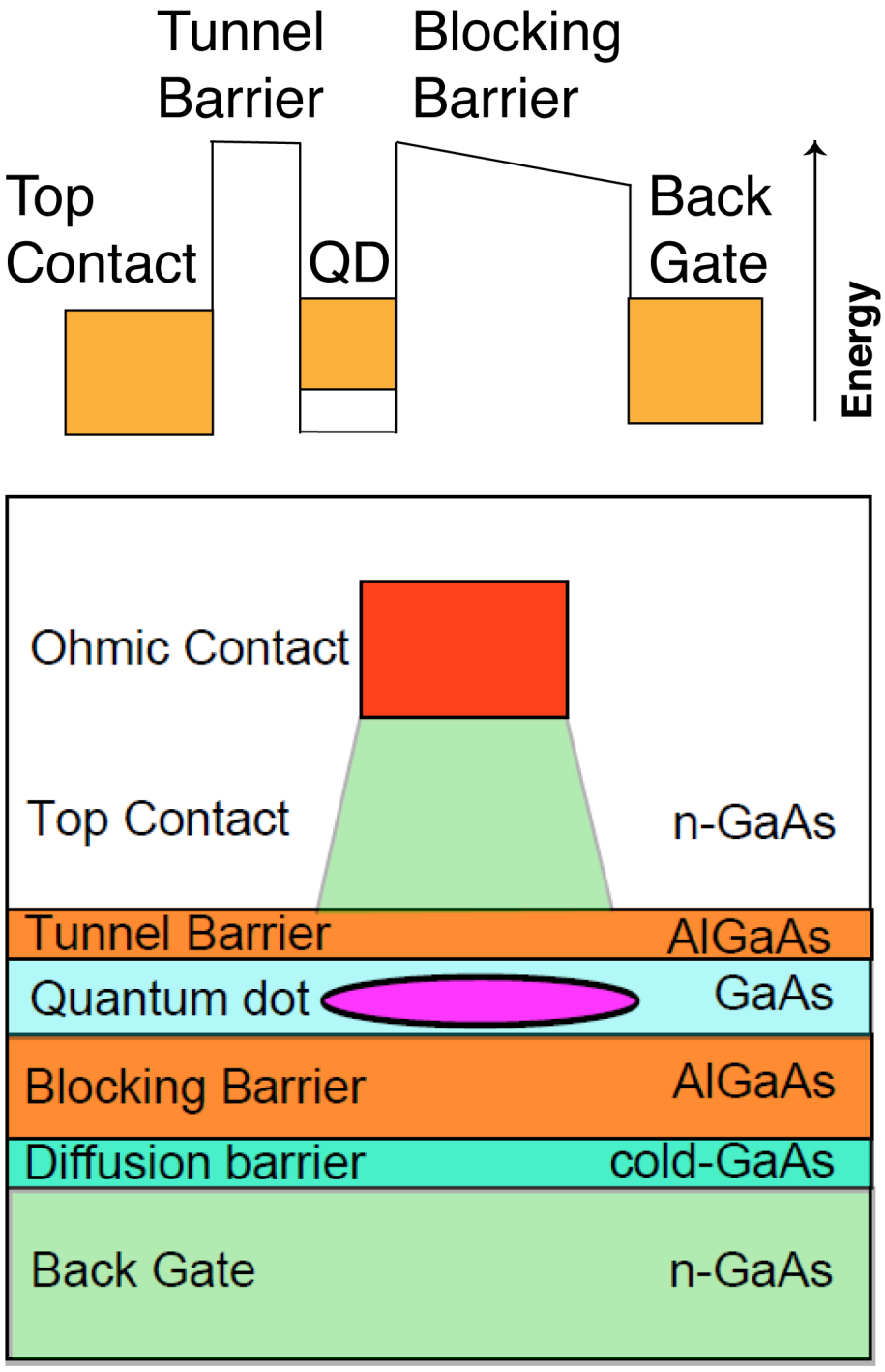


Figure 2-1: MBE growth structure of our vertical capacitance geometry and corresponding band diagram.

this structure the Si dopants in the bottom electrode, which serves as the gate in these structures, are restricted from migrating up into the quantum well by a thin GaAs layer grown at substantially lower temperatures as well as the thick AlGaAs "blocking" barrier.

A schematic of our samples is shown in Fig 2-1. The AlGaAs/GaAs wafer contains the following layers (from bottom to top): 3000 Å $n+$ GaAs electrode, 60 Å GaAs spacer layer, 600 Å AlGaAs blocking barrier, 230 Å GaAs quantum well, 90 Å AlGaAs tunneling barrier, 400 Å GaAs cap layer. A mesa with deep Ohmic contacts down to $n+$ GaAs is initially defined. Then circular Pd/Ge/Au metallic pillars of different size are fabricated on the top of the mesa. Using these pillars as the etch mask, we isolate the dots by plasma etch that stops at first AlGaAs layer. We finalize the dots after making the metallic contact from the pads to the quantum dots.

## 2.2 Measurement Scheme

A schematic of the core experimental setup is shown in Figure 2-2A. The dot is placed between two plates of a parallel plate capacitor. Electron may tunnel back and forth between the dot and the tunneling electrode when the fermi energy is aligned with quantum levels. The experiments consist of observing the image charge resulting from tunneling of single electrons from the metallic contact layer to the levels in the dot as we sweep the gate bias $V_g$: a potential applied across the plates of the capacitor.

### 2.2.1 Capacitance Bridge

In order to sense tiny capacitance changes, we have developed an AC charge sensing technique based on a capacitance bridge. In this technique, we utilize the bridge as in Figure 2-2A where we balance the sample against a known reference capacitor by applying an excitation voltage that is 180 degrees out of phase. The voltage in balance point is nulled when,

$$\frac{\tilde{V}_{exc}}{Z_{sample}} + \frac{\tilde{V}_{ref}}{Z_{ref}} = 0 \tag{2.1}$$

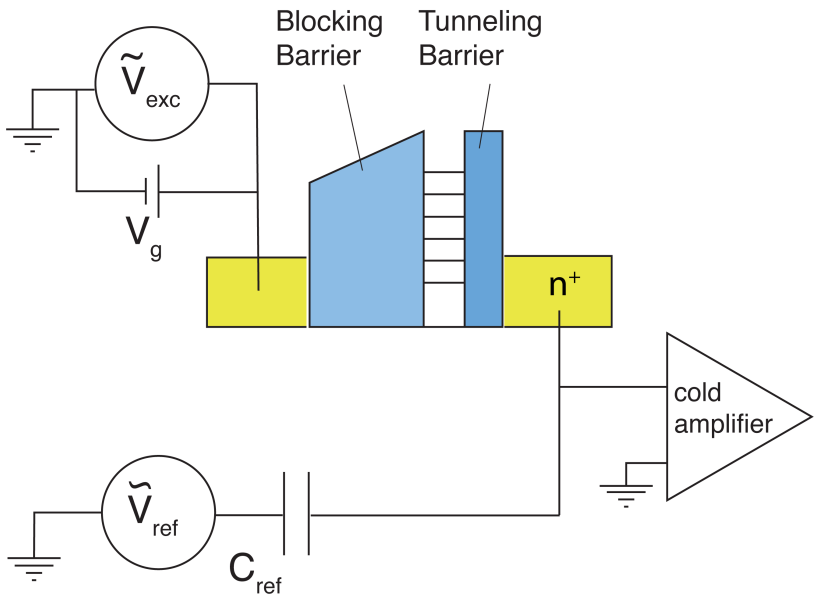


Figure 2-2: Vertical capacitance geometry. The quantum dot is confined between two electrodes one of which (tunneling electrode) is tunnel coupled to quantum dot. The carrier concentration can be tuned by the bias electrode.

where $Z_{ref} = 1/iwC_{ref}$ is the impedance of the reference capacitor and $Z_{sample}$ is the impedance of desired sample. To make a reference capacitor we deposit metal lines on a silicon chip yielding a capacitance of 40 fF. In a purely capacitive circuit, balancing the bridge in this way, the sample capacitance is given by,

$$C_{sample} = C_{ref}\frac{\tilde{V}_{ref}}{\tilde{V}_{exc}} \tag{2.2}$$

The main motivation behind using this technique is to eliminate the effect of constant stray capacitance. Due to wire bonding and the metallic pads in the fabrication process, we have a large stray capacitance in parallel to our devices. Even though we try to minimize the stray capacitance, it remains around 150 fF. Another advantage of the capacitance bridge is that it allows a precise measurement of the sample capacitance without needing an independent measurement of the shunt capacitance or of the gain of any amplifiers.

To balance the bridge, we apply two different excitation voltages to the reference capacitor while applying a known fixed excitation voltage to the sample. Measuring

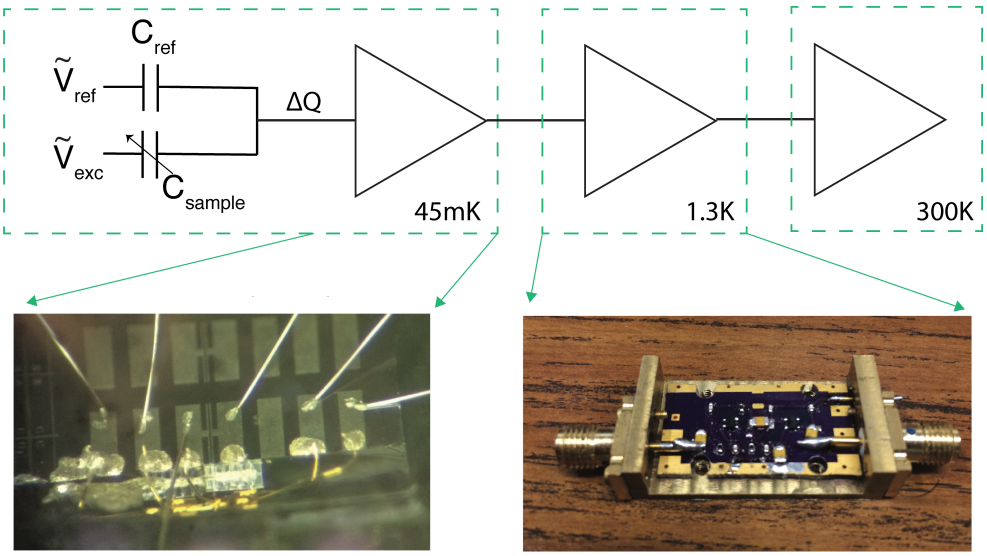


Figure 2-3: Measurement scheme from cryogenic temperatures to the room temperature. The image on the left shows how cleaved transistors are mounted on the edge of a silicon chip. The image on the right shows the 1K Pot amplifier.

the voltage at the balance point for each case, we can then compute the excitation voltages that satisfies the balance condition (Equation 2.1). The capacitance changes are often very small compared to the total sample capacitance. When this is the case, we do not need to balance the bridge at each point. Through out of balance signal, we can directly measure the out of signal and convert that to capacitance.

### 2.2.2 Low Temperature Amplifiers

Since the cables running to the top of the cryostat have a shunt capacitance of at least 300 pF, using a room temperature amplifier to measure the voltage when working with a 50 fF sample capacitance would result in significant signal loss. For this reason, we have designed a cryogenic amplifiers as in Figure 2-3 placed right next to the sample, which allows us to reduce the total bridge capacitance to a value of around 600 fF. The main purpose of this first stage amplifier is to behave as an impedance matcher. We built the cryogenic amplifier using the commercially available high electron mobility transistor (HEMT). The transistors we use are Fujitsu FHX35X chosen[22] amongst many other transistors for their low input capacitance, high transconductance and

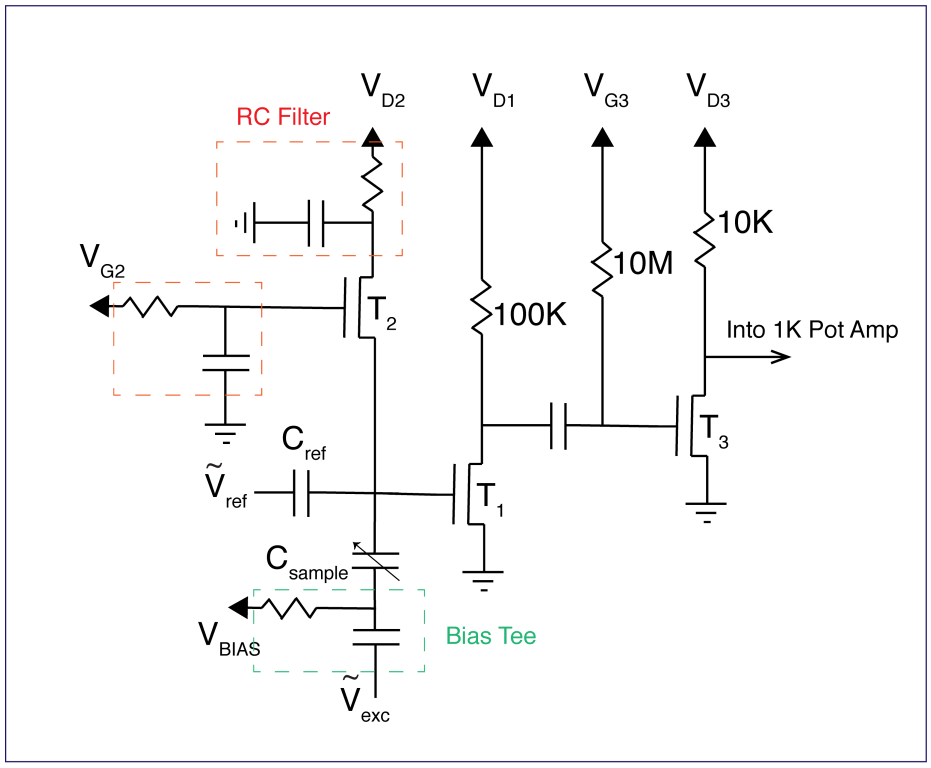


Figure 2-4: The schematic of first stage cold amplifier.

low 1/f noise. Since these transistors are available in an unpacked format, we cleaved the transistors T1 and T2 in Figure 2-4 to reduce the shunt capacitance. When we mount the transistors, we place them vertically on the edge of a cleaved chip as in Figure 2-3 so that during a magnetic field sweep its gain remains unaffected.

The schematic of the amplifier is shown in Figure 2-4. The measurement transistor (T1) is in a common-source configuration receiving the balance point voltage as input. The second transistor (T2) is the bias transistor. By pinching off the channel at T2, we use it as a high impedance resistor to gate T1 transistor. It is unconventional to use transistors as resistors, however the only other alternative is long meander line resistors. These resistors add a shunt capacitance as much as 1pF reducing our electron sensitivity. While DC biasing the bias transistor T2, we realized the DC lines for $V_{G2}$ and $V_{D2}$ carry substantial amount of noise which causes input overload in the lockin amplifier. As a result, we are utilizing simple RC filters to reduce that

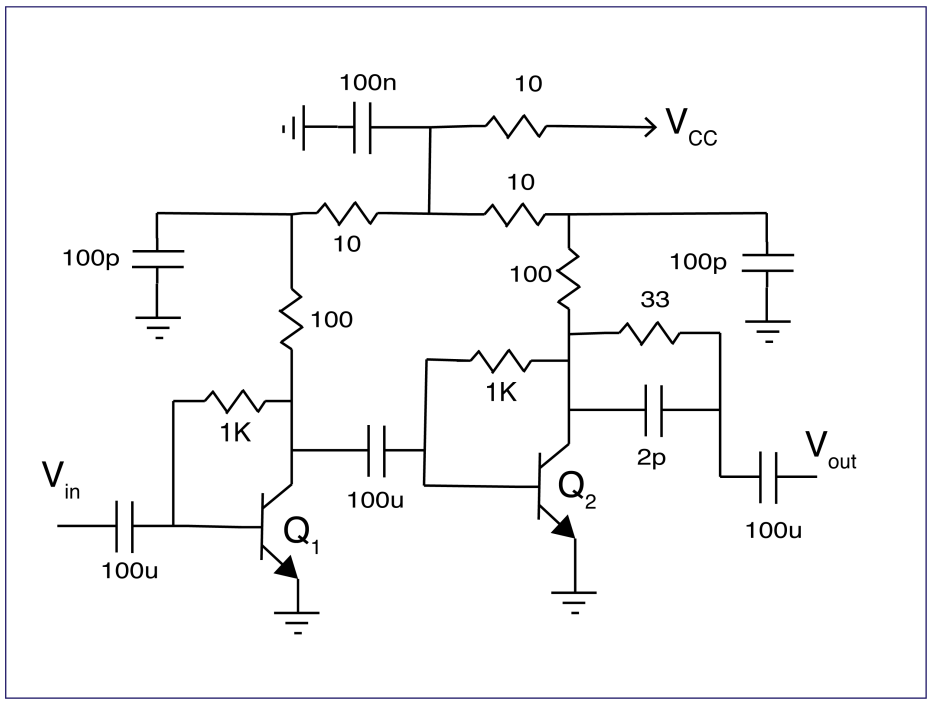


Figure 2-5: The schematic of 1K Pot cold amplifier.

noise. This modification increased our sensitivity significantly.

Noise in the experiment comes mostly from the intrinsic noise of the HEMT transistor, ground loops or unshielded cables. The HEMT transistors have an intrinsic noise spectrum that has a 1/f character, and that is characterized as fluctuations in the channel conductance. Because the noise diverges at low frequencies, there is a significant advantage to working at high frequencies. The noise becomes qualitatively bad below about 10 kHz, and makes it impractical to measure single electrons below this frequency. At 240 kHz, with a well optimized setup, we have achieved input noises as small as $5\,\mathrm{nV}/\sqrt{\mathrm{Hz}}$.

### 2.2.3 1K Pot Amplifier

The cryogenic first stage amplifier shown in Figure 2-4 will suffer from a poor bandwidth due to a large capacitance from the cable(roughly 300 pF) connected to its drain to the room temperature. The output of T3 must charge up this capacitor through the impedence of load resistance. To circumvent this problem, and to add additional

amplification that is operating at cold, we are using a low noise cold amplifier staged at 1K Pot of the cryostat. We use two stage amplifier using commercially available, very high performance silicon germanium bipolar transistors (NXP BFU725). The original design[29] is a band-pass filter with low cut-off frequency at 500 MHz. By adjusting the shunt capacitors in Fig 2-5 to 100 µF we were able to reduce this frequency to tens of Hz. The advantages of this 1K Pot amplifier is that it has good input impedance match and flat gain over a decade of bandwidth extending to low frequencies, and it has stable operation point.

## 2.3 Capacitance Step

In this section, we discuss the capacitance of our devices and the characteristics of the tunnel barrier. The tunnel barrier can be modeled as a simple resistance($R_t$) and capacitance($C_t$) in parallel. Hence, the equivalent circuit schematic for vertical quantum dots, as in Figure 2-6A, can be thought as the tunnel barrier being in serious with a capacitance $C_{blocking}$.

Due to RC equilibration time at the tunneling barrier, the capacitance of quantum dots becomes also a function of frequency. At low frequencies, there is sufficient time during one cycle of the measuring voltage for a full electron charge to be transferred between the tunneling electrode and the quantum dot. In our measurements, we are usually working in the low frequency regime. In Figure 2-6C, we are presenting the capacitance of a large quantum dot as a function of gate voltage. The dot is completely depleted for bias voltages less than $V_{Bias} = -0.1\,\mathrm{V}$. The capacitance measured at the depletion region is effectively the geometric capacitance between the two electrodes. With gating, we can populate the quantum dot with electrons. At this point, we now have available states to tunnel into. Since we are measuring the capacitance at the low frequency regime, the tunneling electrode will be well coupled to the quantum dot. As a result, we observe an increase in the capacitance of the dot. These two extreme cases are simply illustrated in Figure 2-6B. For a large quantum dot, where the shunt capacitance is negligible compared to sample capacitance, the

capacitance can be simplified to,

$$C_{sample} \rightarrow \begin{cases} C_b \frac{1}{(1+\frac{C_b}{C_t})}, & depletion\, region \\ C_b, & dot\, populated \end{cases} \tag{2.3}$$

The sharp rise in Figure 2-6C in the low frequency capacitance data occurs as the gate bias is increased beyond the threshold which allows electrons to enter the quantum well. This capacitance step develops as electrons from the $n+$ layer fill up the quantum well, reducing the effective distance between the capacitor plates. From these data we extract the level arm to be $\eta = 4$. The sharpness of the capacitance step is only 50 mV, is a signature of cleanliness of our devices.

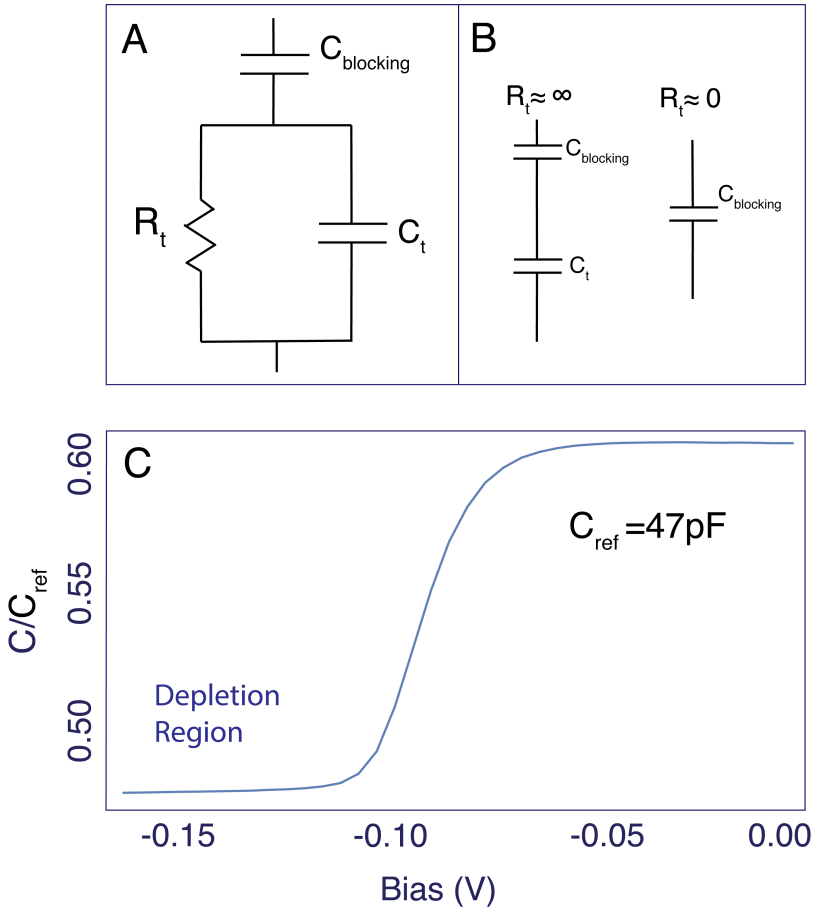


Figure 2-6: (A) Equivalent circuit diagram of the sample. (B) Equivalent circuit diagram in the low frequency regime when the dot is depleted vs populated. (C) Capacitance of a single quantum well as a function of bias voltage. When the well is populated, the tunneling electrode becomes coupled to the well which results in a capacitance step. Excitation voltage is $V_{exc} = 1\,\mathrm{mV}$.

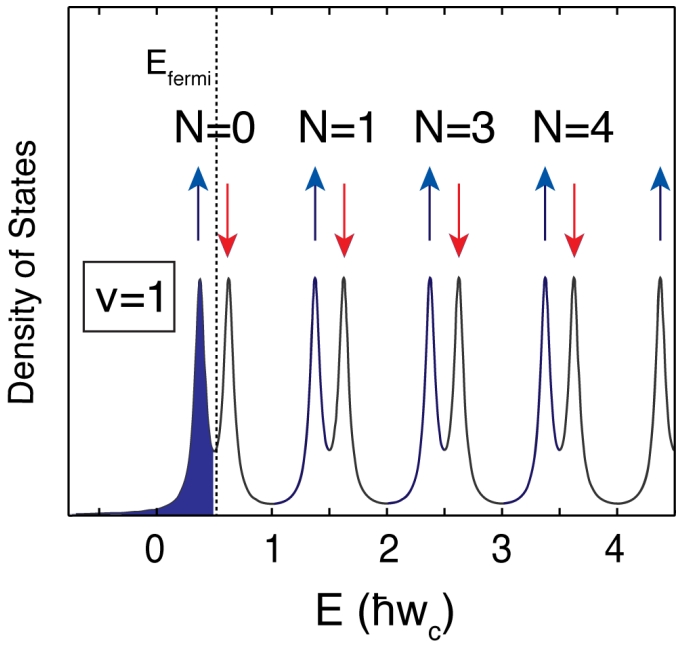


Figure 2-7: The density of states of an interacting electron gas at filling fraction $\nu = 1$.

### 2.3.1 Landau Level Formation

Under the presence of an external magnetic field, particles in a quantum well have quantized cyclotron orbits. As a result, the particles can only occupy orbits with discrete energy values, called Landau levels. Conventionally, the density of a two-dimensional electron gas is described in terms of the filling fraction which is defined as the number of available electrons per landau level degeneracy. Because of the additional spin degree of freedom, the filling fraction is $\nu = 2$ when the first orbital level is filled, $\nu = 4$ when the second level is filled, etc. At $\nu = 0$, there are no electrons in the 2DEG.

At $\nu = 1$(Figure 2-7), we have populated the well with enough charge to fill one spin-state of the N = 0 Landau level. These states are degenerate before we turn on electron-electron interactions. Due to the formation of an exchange-enhanced spin gap, as we fill the quantum well, the interaction causes the electrons to spin-align. At $\nu = 1$, the spin up states of N = 0 are completely filled and lie below the Fermi energy, while the spin down states are completely empty and lie above the Fermi energy.

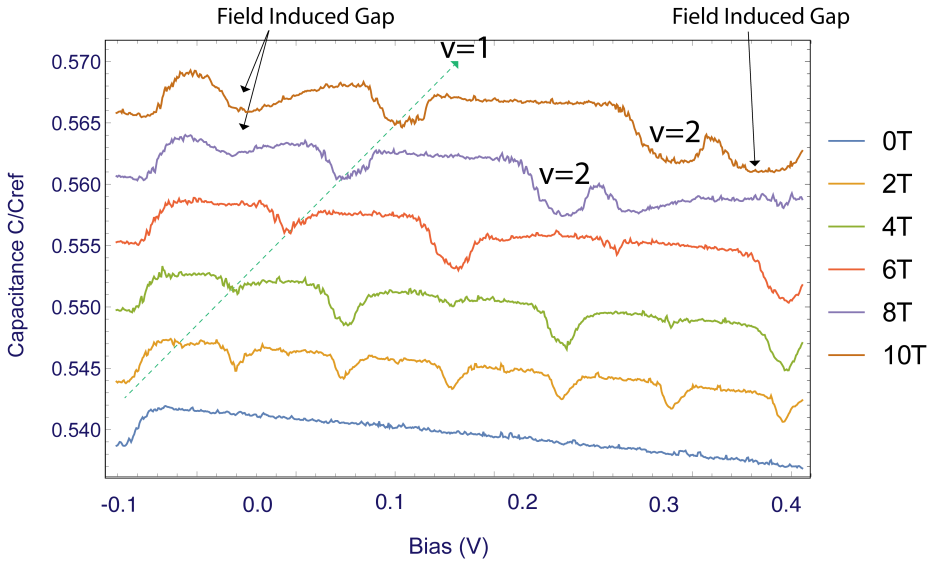


Figure 2-8: Capacitance sweeps starting from 0T to 10T. The measurement frequency is 50KHz. Excitation voltage is $V_{exc} = 1\,\mathrm{mV}$.

In capacitance measurements, we are sensitive to the compressibility of the quantum well. A capacitance gap develops whenever the density of states goes to zero. In Figure 2-8, we present capacitance sweeps taken at different magnetic fields from 0T to 10T. At zero magnetic field, we simply observe a capacitance step. As we increase the magnetic field, we allow landau levels to be formed. At B=2T, the landau level gaps are clearly formed, and also the exchange interaction begins to lift the degeneracy of N=0 landau level. At high fields, we also observe a suppression of tunneling to the bulk.

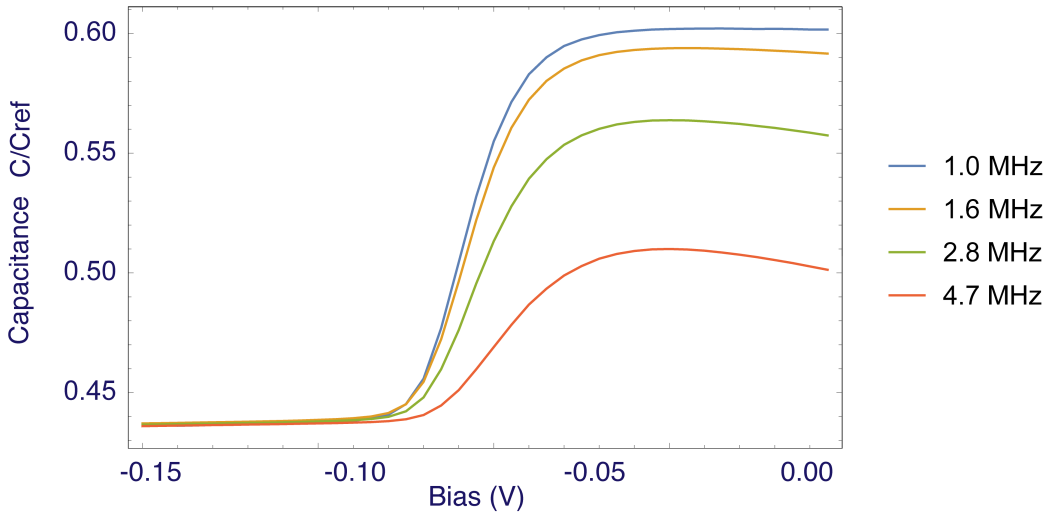


Figure 2-9: Frequency response at zero magnetic field. We see a suppression of capacitance only above 4 MHz. The tunneling barrier is transparent to our common measurement frequencies which is usually below 1 MHz. Excitation voltage is $V_{exc} = 1\,\mathrm{mV}$.

## 2.4 Frequency Response of the Tunnel Barrier

At high frequencies, there is insufficient time during one cycle of the excitation voltage to fully drive the charge to the quantum dot. Because of RC equilibration time, the capacitance at high frequency is lower than its low frequency value. The frequency where the capacitance is significantly suppressed is defined as the roll-off frequency.

In a typical tunneling measurement, the roll-off frequency depends on the tunnel barrier and the density of states in the electrode and in the quantum dot. We observe different tunneling rates in zero field and in magnetic field. In the following sections, we are trying to figure out the roll-off frequency in two extreme cases.

The tunnel barrier thickness was designed so that the mean time for an electron to tunnel between the $n+$ layer and the well is less than $1\,\mu$s. During one cycle of the excitation charge can tunnel many times back and forth through the barrier.

In Figure 2-9, we present zero field capacitance data taken at different frequencies. In this measurement, we aim to find out the roll-off frequency at which the capacitance step is suppressed significantly. Starting from $f = 1\,\mathrm{MHz}$, sweeping up to $f = 4.7\,\mathrm{MHz}$, we begin to observe a capacitance suppression. Mainly, what Figure 2-9

tells us is that, in zero magnetic field, electrons can tunnel back and forth in phase with the excitation through the barrier if the measurement frequency is below 1 MHz. Most of the data in this thesis has been taken at $f = 247\,\mathrm{KHz}$ indicating that we are in the low frequency regime.

In Figure 2-10, we present a capacitance sweep taken at fixed magnetic field, B=10 T, for different frequencies ranging from 6.2 KHz to 100 KHz. We begin to populate the dot at $V_{BIAS} = -0.10\,\mathrm{V}$. Near $V_{BIAS} = 0.15\,\mathrm{V}$, all carriers fall into the spin polarized landau level $\nu = 1$. What is striking in Figure 2-10 is the suppression of capacitance, at f=50 KHz and f=100 KHz. This indicates that the ac excitation frequency is higher than the roll-off frequency at B=10 T. In other words, the period is shorter than the RC relaxation time of the tunnel barrier. The suppression in the capacitance data comes from tunneling anomaly near Fermi energy induced by magnetic field[30]. At high magnetic field, the tunneling is suppressed for states near the Fermi energy. Unlike the gaps associated with fractional quantized Hall effect which happens at particular densities, magnetically induced gap is tied to Fermi level. Hence, we observe a broad tunneling suppression in the capacitance data.

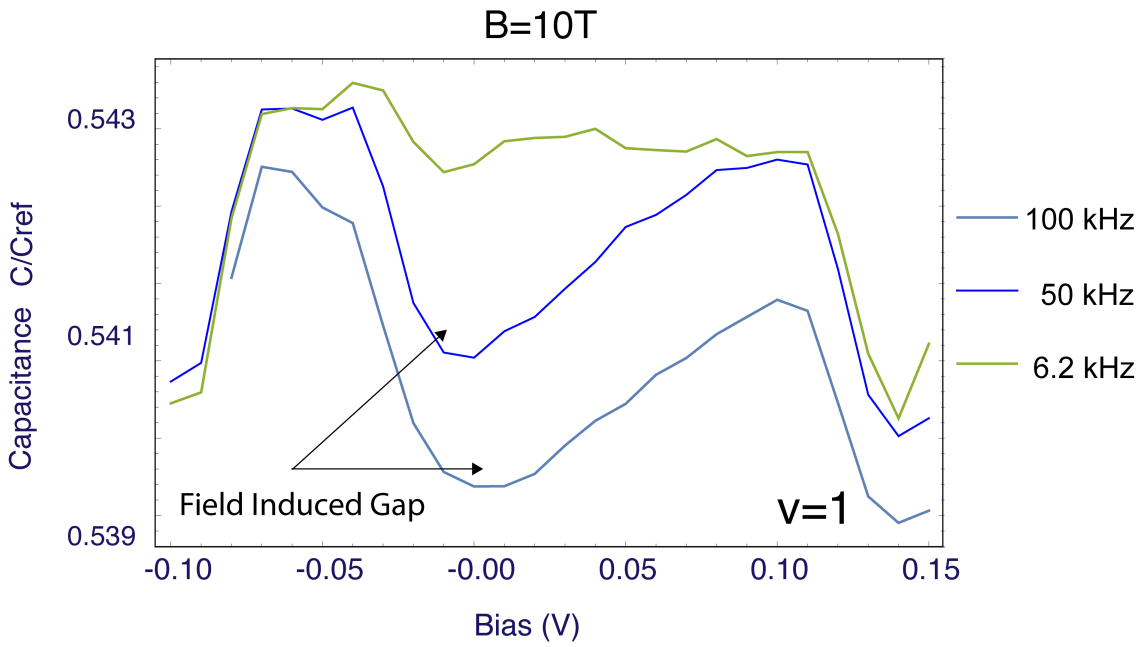


Figure 2-10: Capacitance sweep at B=10T for different frequencies. At high fields, the tunneling rate gets slower than zero field. We observe a suppression at near f=20KHz. This suppression is caused magnetic field induced gap.

## 2.5 Single Electron Additions

In Figure 2-11, we observe a sequence of well resolved and reproducible capacitance peaks. In our tunnel capacitor, near an isolated capacitance peak, at most one electron is induced to tunnel between the $n+$ layer and the discrete state in the well. The electron travels only a fraction, $1/\eta$, of the distance between the plates of the tunnel capacitor. Therefore, the amount of charged induced on the gate due to a single electron tunneling is $e/\eta$, which translates to a voltage change at the balance point of $e/\eta C_{shunt}$. The level arm, $\eta$, is determined to be 4.0 from the MBE growth parameters and capacitance measurements on large area dots. The lever arm also sets the reduction factor between externally applied voltage and the voltage drop between the $n+$ layer and the quantum well.

The Coulomb blockade peak position as a function of gate voltage reflects the electrochemical potential of the dot. Then, the addition energy - the separation between the two nearest Coulomb blockade peaks - is given by the following expression:

$$\mu_{dot}(N+1) - \mu_{dot}(N) = E(N+1) - E(N) + e^2/C, \tag{2.4}$$

where E(N+1) and E(N) are sequential single particle states. Here we assume that $C$ is independent of the number of electrons on the dot. Electrons simply fill single particle states additionally separated by a constant charging energy $\Delta E_c = e^2/C$. In Figure 2-11, we show single capacitance peaks for a dot that has diameter around 120 nm. Since the dominating energy scale is the charging energy, the electron peaks are mostly evenly spaced by charging energy. This trace is probably the best capacitance data we have taken with clearly visible isolated capacitance peaks.

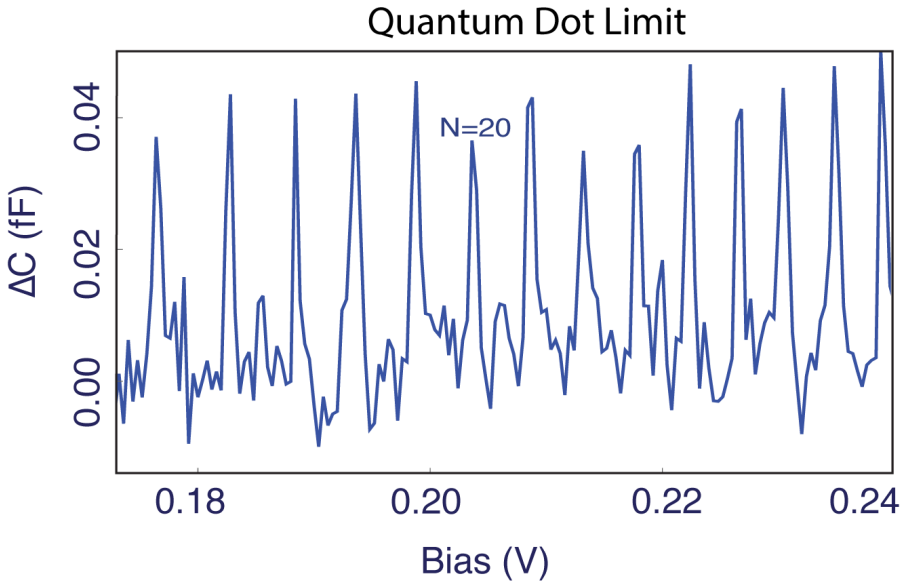


Figure 2-11: Capacitance peaks as a function of the bias voltage. Each peak corresponds to an electron addition to small quantum dot.

## 2.6 Electron Temperature

In this section, we will extract the electron temperature using the broadening of a single electron peaks. Consider DC bias $V_0$ to be set at the center of an isolated capacitance peak. Then, added a small excitation $V_{exc} = v\cos wt$, the net voltage over the tunnel capacitor becomes $V_{sample}(t) = V_0 + v\cos wt$. The likelihood of the occupation of that single electron level is given by Fermi distribution, $f(V_{sample})$. The voltage change at the balance point due to a tunneling event is Fermi distribution function multiplied with $e/\eta C_{shunt}$[27].

During one cycle of the excitation, an electron can tunnel many times back and forth through the barrier. We choose an AC frequency much lower than the roll-off frequency of the tunnel barrier so that we operate in the low-frequency limit. For instance, in the zero temperature limit, the quantum level in the dot tends to be occupied during positive portions of the AC excitation and unoccupied during negative portions creating a square wave signal at the balance point. Depending on how far the DC voltage is from the center of the peak, what we measure in the lockin is the variable duty cycle square wave amplified through the cold amplifiers. The lock-in amplifier picks up the Fourier coefficient of this voltage at the excitation frequency $w$. Equations 2.5 and 2.6 below were previously described at Ashoori et al[27].

$$V_{lockin}(V_0) = A_v \frac{we}{\sqrt{2}\pi\eta C_{shunt}} \int_0^{2\pi/w} f(V_0 + v\cos wt)\cos wt dt \tag{2.5}$$

where $A_v$ is the total gain from the balance point to the input of lockin. The division by $\sqrt{2}$ is made because the lock-in reads the rms amplitude of the Fourier coefficient. A change of variables, $U = V_0 + v\cos(wt)$, and integration by parts yields

$$V_{lockin}(V_0) = A_v \frac{\sqrt{2}e}{\pi\eta C_{shunt}} \int_{V_0-v}^{V_0+v} \frac{df(U)}{dU} \sqrt{1 - (\frac{V_0 - U}{v})^2} dU \tag{2.6}$$

At zero temperature, the derivative, $\frac{df(U)}{dU}$, is simply given by $\delta(U - V_n)$ , where $V_n$ is the sample voltage at which the $n$th electron enters the dot. Therefore the

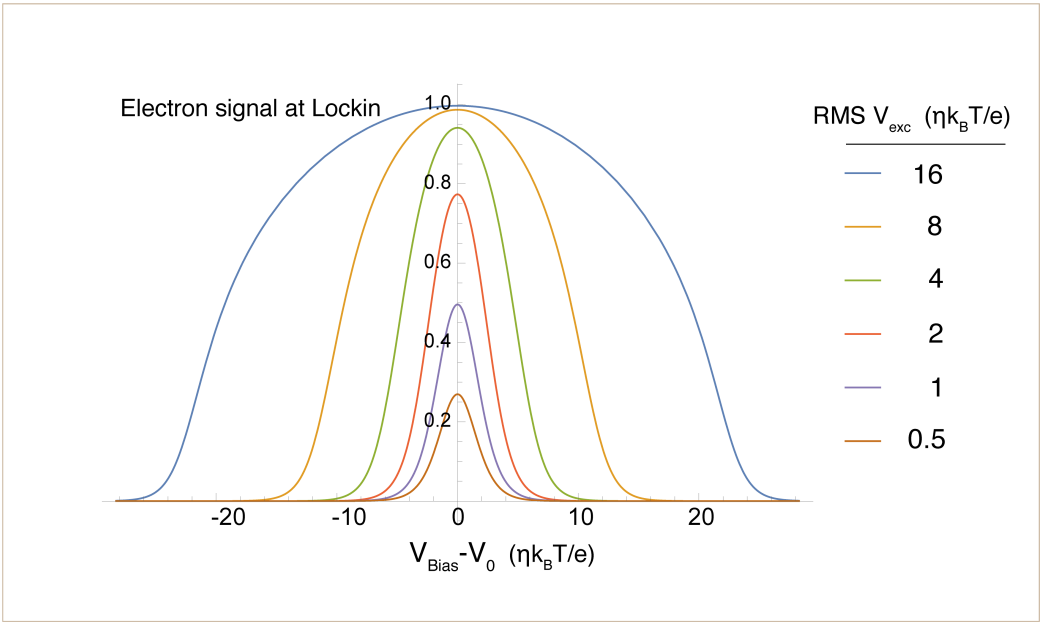


Figure 2-12: Simulation of the voltage response of an electron addition to AC excitations of varying amplitude

expected response at the lock-in is half an ellipse of height $A_v \frac{\sqrt{2}e}{\pi\eta C_{shunt}}$ with base width of twice the amplitude of the AC excitation, centered at the sample voltage $V_n$. At nonzero temperatures, and for $v < \eta k_B T/e$, the height of the peak drops and becomes amplitude dependent. For $v \gg \eta k_B T/e$, the peak height saturates at $A_v \frac{\sqrt{2}e}{\pi\eta C_{shunt}}$, and only its width increases.

In order to understand this behavior, in Figure 2-12, we simulated the voltage response of an electron addition to AC excitations of varying amplitude. On the y-axis we present the normalized response at the lockin with respect to maximum response $A_v \frac{\sqrt{2}e}{\pi\eta C_{shunt}}$. The RMS value of the AC excitation is varied from $0.5\eta k_B T/e$ to $16\eta k_B T/e$. In each subsequent curve the excitation amplitude increases by a factor of 2. On the x-axis, we sweep the applied DC voltage around the center of the peak $V_0$.

Figure 2-12 shows that for $v_{rms} \gg \eta k_B T/e$, the peak height saturates the maximum value, and only its width increases. For $v_{rms} < 4\eta k_B T/e$, the height of the peak

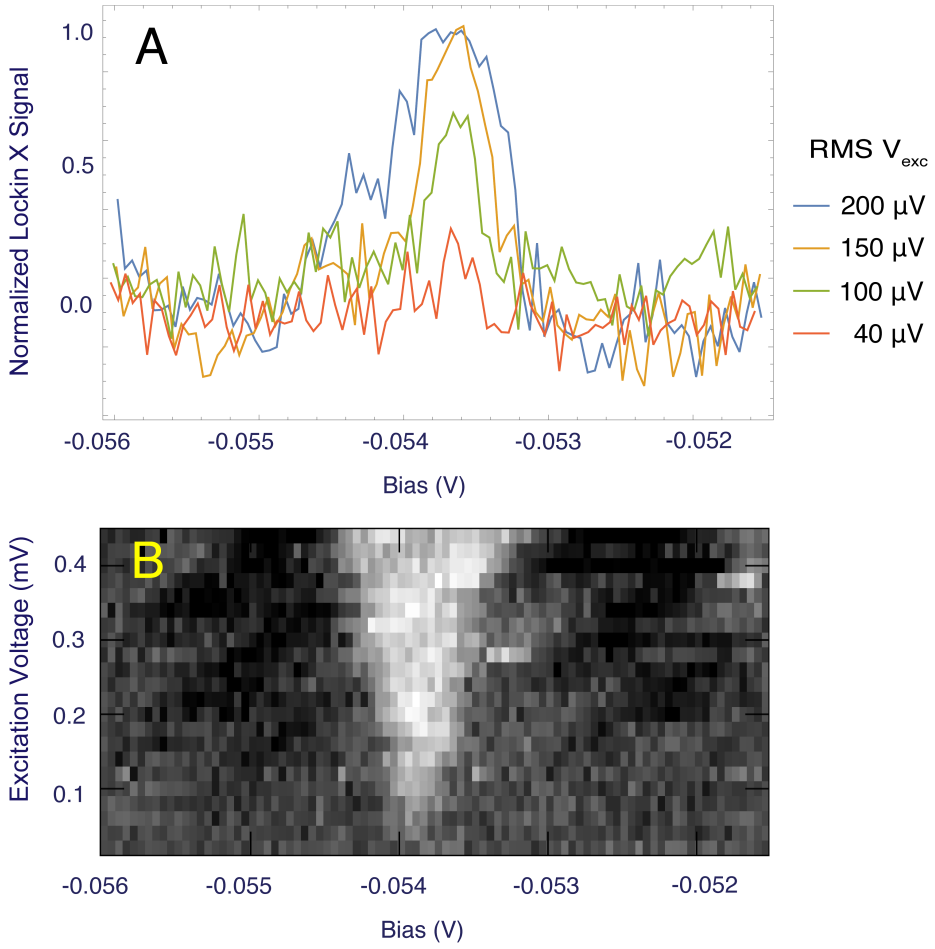


Figure 2-13: Measured Lockin Signal at varying excitation voltage.

drops and becomes amplitude dependent. The full width at half maximum height stays constant at roughly $4\eta k_B T/e$. As clearly shown in Figure 2-12, to get maximum voltage response we need to drive the tunnel capacitor with an AC excitation greater than $v_{rms} = 4\eta k_B T/e$. Above this excitation voltage, the peaks broaden. However, below this excitation voltage we will lose the signal height.

Our experimental data from a single isolated capacitance peak(sample QD-23-1-5) is shown in Figure 2-13. To get an estimation of electron temperature, we can observe two things. The excitation voltage at which the voltage response is significantly lower than the maximum response is roughly $4\eta k_B T/e$. The peak width

at the lowest excitation which we can still observe a height is also roughly $4\eta k_B T/e$. Looking at the amplitude that is measured at lockin, we observe that below excitation voltage $V_{exc} = 100\,\mu$V, peak height starts to drop. Therefore this gives a temperature estimation of ($4\eta k_B T/e = 100\,\mu$V) 72mK. This is slightly warmer than the dilfridge base temperature 45mK. It is likely that the power dissipated by the transistors heats the sample. In Figure 2-13B, we observe that the peak width increases linearly with the excitation voltage above $60\,\mu$V. Below that excitation, we lose the electron resolution probably due to low signal to noise ratio.

THIS PAGE INTENTIONALLY LEFT BLANK

# Chapter 3

# Small Quantum Dots

## 3.1 Introduction

Probing of the energy levels and density of states as a function of magnetic field and density is the natural method to determine the electronic state of a quantum dot. Previous measurements on electron addition spectroscopy of quantum dots show well defined transitions into the integer quantum Hall states, indications of possible fractional states as the dot transitions from the spin-polarized maximum density droplet at $\nu = 1$ to lower density droplets at $\nu < 1$[20, 21, 17, 18].

In the previous chapter, we have learned how to detect single electron additions to a quantum dot using capacitance technique. Improving the signal sensitivity and sample quality in comparison to Ashoori group's previous work[22], in this chapter we present the capacitance measurements starting from small size quantum dots. Most of the data in this chapter is taken by former postdoc, Neal Staley.

## 3.2 Single Particle Spectrum

To illustrate the functioning of the capacitance method and the low disorder of the quantum dots, we first show data from a small dot that has a diameter of $\sim 120\,\mathrm{nm}$. Electron additions occur periodically in gate voltage with roughly a period $e/C_g$, where $C_g$ is the capacitance between the gate and the dot. After each electron is

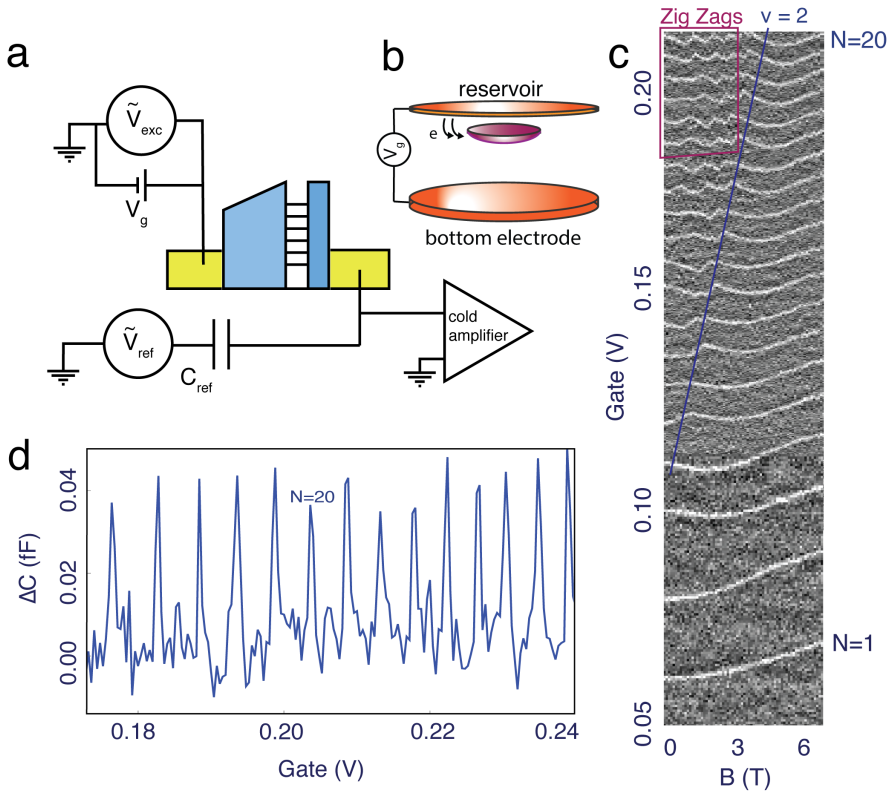


Figure 3-1: Vertical capacitance geometry and single electron additions to a quantum dot. **a**, The quantum dot is confined between two electrodes, one of which (tunneling electrode) is tunnel coupled to quantum dot. The carrier concentration can be tuned by the gate electrode. Using a capacitance bridge, we balance the sample capacitor against a known reference capacitor. **b**, The schematic of a small metallic island that is coupled to a reservoir and a gate electrode. **c**, Single electron capacitance peaks in a small quantum dot as a function of external magnetic field and gate voltage. For electron numbers $N > 15$, "zig-zags" appear in the traces arising from the lowest energy available electronic state shifting between the interior and the edge of the dot. **d**, Isolated electron additions as a function of gate voltage. The spacing between successive capacitance peaks largely reflects the additional energy required to overcome the Coulomb repulsion of the existing electrons in the dot.

added to the dot, adding a successive electron requires increased gate voltage due to Coulomb repulsion[31, 32, 21, 24]. Figure 3-1, presents capacitance data taken from a small dot in a dilution fridge with 45mK base temperature. These data show electron additions from $N = 1$ to $N = 20$ under an external perpendicular magnetic field show features that fit with a model of a small quantum dot with a parabolic confining potential[33, 34]. As the gate voltage is sweeped on the y-axis, capacitance peaks appear for every electron that enters to the dot. Note that the lateral extent of electrons in the dot gradually increases with electron number, decreasing the observed spacing.[21] The first dozen electron additions can be bunched into groups of two electron additions, with each group of two showing very similar behavior in magnetic field, in agreement with a simple model in which electron states are occupied by two electrons with opposite spin states. The dotted line shows the density and B value at which all electrons occupy spin-degenerate states belonging to the lowest orbital Landau level ($\nu = 2$ in a 2DEG).

The spacing between the capacitance peaks in Figure 3-1d reflects the energy to add one more electron to a dot containing N electrons. The experimental spectra shows electronic states are well separated by Coulomb blockade. In Figure 3-1c we observe many features of a noninteracting electron model with an additional charging energy. The energy spectrum in a B field aligned with positive z axis can be solved analytically for a dot with a harmonic confining potential[33, 34]. The energy $E_{nl}$ of a state with a radial quantum number $n = 0, 1, 2, ...$ and angular momentum quantum number , $l = 0, \pm 1, \pm 2, ...$ is given by

$$E_{nl} = (2n + |l| + 1)\hbar(\frac{1}{4}\omega_c^2 + \omega_0^2)^{1/2} + 1/2l\hbar\omega_c \tag{3.1}$$

where $\hbar\omega_0$ is the electrostatic confinement energy and $\hbar\omega_c$ is the cyclotron energy. The calculated spectrum for $\hbar w_0 = 4\,\text{meV}$ is given at Figure 3-2. States of positive $l$ correspond to electrons moving anticlockwise as viewed looking down from positive z axis, negative $l$ states move in the opposite direction. Therefore positive $l$ states have magnetic moment pointing opposite to applied magnetic field whereas negative $l$

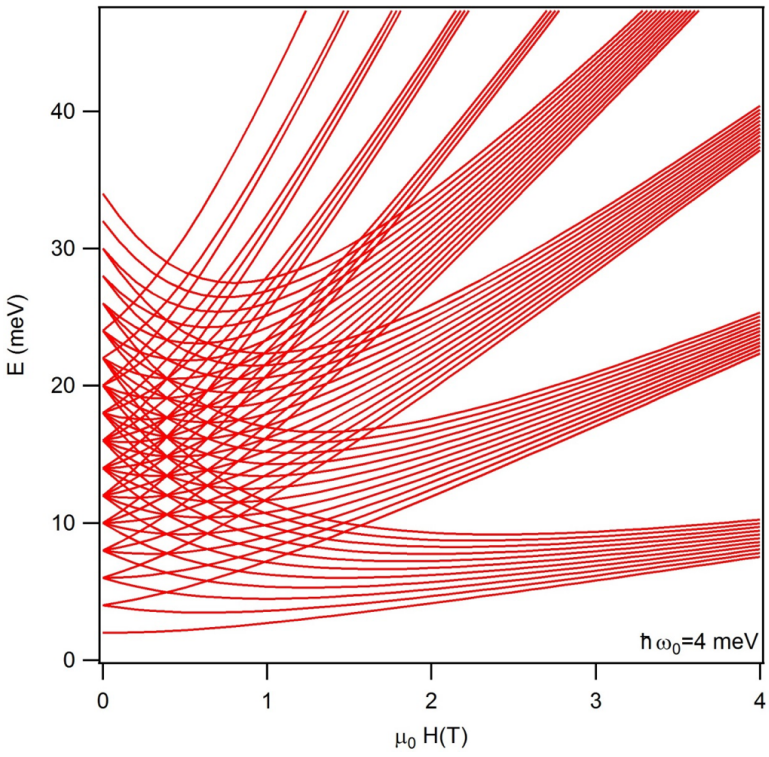


Figure 3-2: Spinless Fock-Darwin spectra for given n and l. At given chemical potential, the highest energy electron will have zig zags every time there is a crossing of different states.

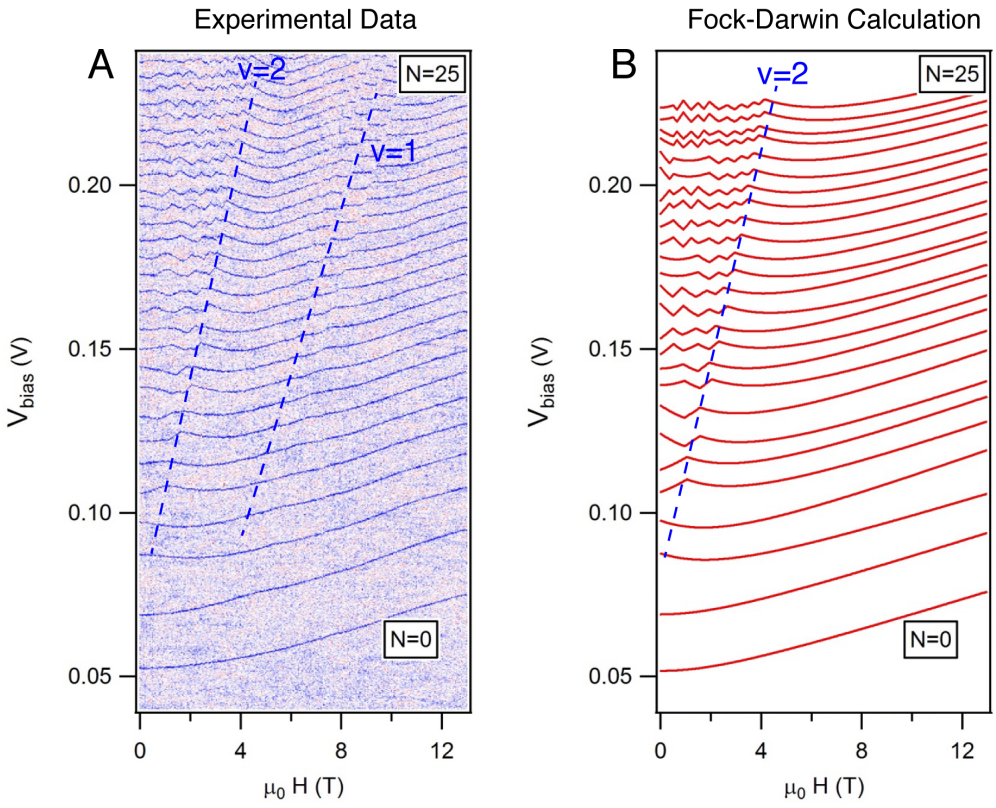


Figure 3-3: (A) Capacitance peaks of a small quantum dot. Low magnetic fields fit well to a Fock-Darwin Hamiltonian. (B) Fock-Darwin calculation for electron additions to a small quantum dot under external magnetic field.

states have magnetic moment aligned with magnetic field. As a result, with increasing magnetic field electrons with negative $l$ states will have lower energy than the rest. Consequently the electrons with high energies will fall into lower energy states.

The "zig-zags" in the evolution of the single particle peaks with magnetic field indicate crossings of energies of single-particle states. As the magnetic field increases, the energies of the edge states move down relative to the states in the bulk since their orbital magnetic moment is aligned with the field[20]. At the crossovers of different states, the highest energy electron tracks the state that is energetically lower. Consequently, the peak position is expected to zig and zag as the highest energy electron moves from one state to another. The zig-zag behavior ends when all electrons fall into lowest Landau level, at filling factor $\nu = 2$.

The calculated ground state spectrum including a degeneracy of two for the electron spin is given in the Figure 3-3B. This spectrum fits the experimental data well in Figure 3-3A. Single particle states calculated here are have the simplest symmetric parabolic confinement shape. In real systems, electrons present in the dot modify the bare confinement potential significantly due to screening. The resulting potential has a flattened bottom in the regions of nonzero electron densities[35].

We observe deviations from single particle picture due to electron-electron interactions. First, due to exchange interactions, at low densities we observe singlet to triplet transitions similar to work done by Tarucha et al. [17]. And at high magnetic field, we observe discontinuous electron additions near filling factor $\nu = 1$, similar to work done by Ooesterkamp et al. [18].

## 3.3 Maximum-Density Droplet and Charge Redistributions

When all electrons are fallen into spin unpolarized state $\nu = 2$, increasing magnetic field spin polarizes the dot, and compresses the droplet. At high magnetic fields over a region of the charge density, the electrons are spin polarized near $\nu = 1$. This is the maximum-density-droplet (MDD) state[36] in Figure 3-4. The stability of this state is determined by the balance of different forces such as Coulomb interaction, confining potential, and exchange interaction[36]. When the magnetic field is increased even

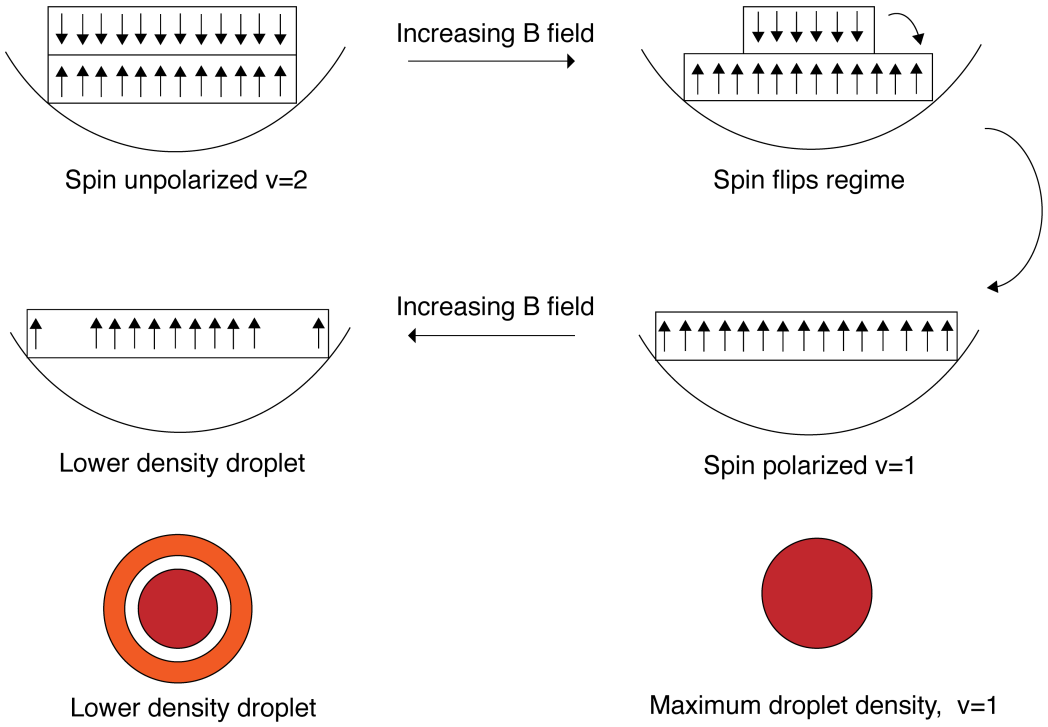


Figure 3-4: Wedding cake picture. When all electrons are fallen into spin unpolarized state $\nu = 2$, increasing magnetic field spin polarizes the dot. The maximum density droplet state is when all electrons are at spin polarized state $\nu = 1$. At lower density droplet, we believe that abrupt changes happen in the charging configuration resulting in discontinuous behavior near filling factor $\nu = 1$.

further, the density of electrons also grows. As a result, the total Coulomb energy increases due to Coulomb interaction. Therefore, in order to minimize the total energy, the droplet goes through charge reconfiguration as in Figure 3-4.

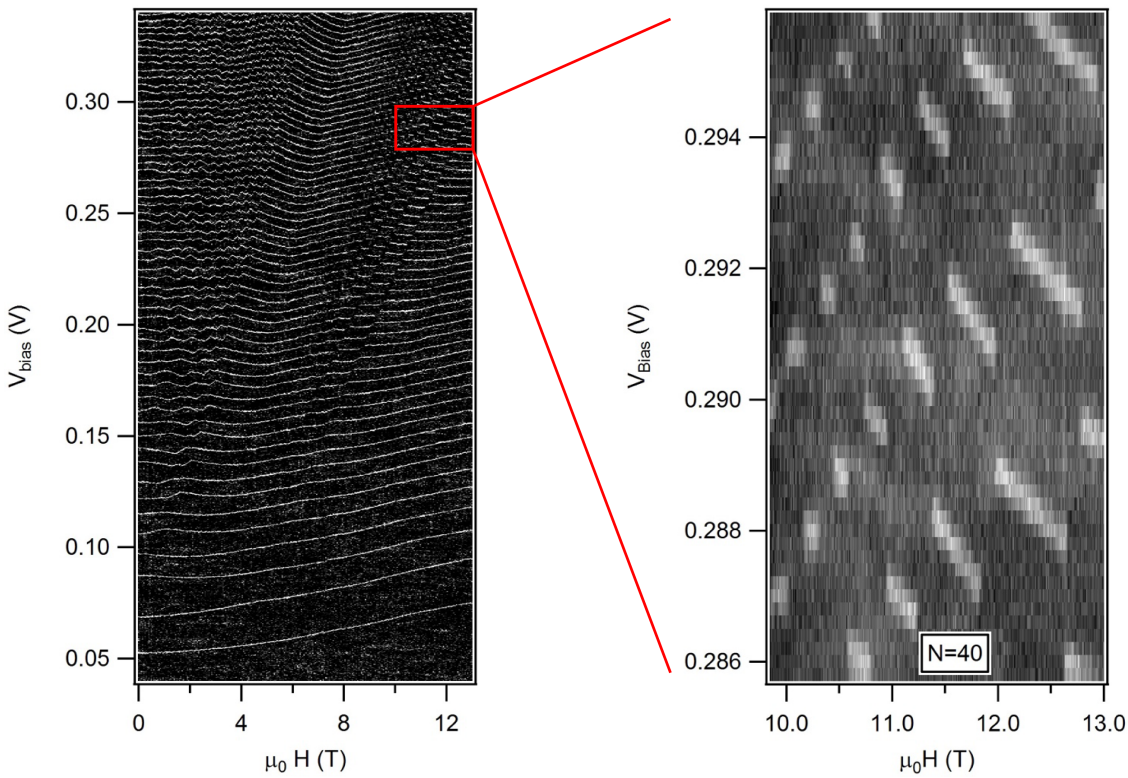


Figure 3-5: Near filling factor $\nu = 1$, we observe discontinuous electron additions to a QD.

Figure 3-5 shows that as we change the magnetic field, and the number of electrons, we observe numerous discontinuities and in particular regions a large suppression in the tunneling rate. These discontinuities cannot be explained in the single particle picture. In applying a very small AC excitation, the highest energy electron moves across the tunneling barrier back and forth. At high magnetic fields, near filling factor $\nu = 1$, these discontinuities suggest that there is a large suppression in the tunneling of electrons. The addition of last electron to the QD lowers the configuration energy preventing the last electron to be removed from the QD. Using higher AC excitations, electrons have enough energy to overcome this barrier. In Figure 3-6 and 3-7, we present the data using higher AC excitations. Here, in Figure 3-6, we observe that the discontinuous lines become continuous, because electrons have sufficient energies to overcome the energy barrier that is resulted from charge reconfiguration.

Oosterkamp et al.[18] saw similar behavior in previous transport measurements through a vertical quantum dot. They attribute all these jumps to abrupt charge redistributions of the droplet in the lower density droplet. In the simplest toy model, if the addition of a new electron to a quantum dot containing $N$ electrons necessitates a major shift in the ground state arising from a "reconstruction" of the quantum dot edge. Therefore the unreconstructed $N$ electron system plus one electron has small overlap with final $N+1$ electron ground state, leading to a reduced tunneling rate for small excitations. While Oosterkamp et al. used a vertical quantum dot geometry somewhat similar to ours, it differed in that they had tunnel barriers to tunneling electrodes (source and drain) above and below the dot, respectively, and they made measurements on the dot by sending currents through the vertical quantum dot. For ground state measurements, current was measured in response to a small dc drain source voltage. When an electron hops from the drain to $N$-electron system, it can hop out to the source easily if it doesn't result in abrupt charge reconfiguration. For a range of magnetic field and gate biases the addition of a new electron causes edge reconstruction, the new $N+1$ ground state diminishes the tunneling probability and yields a suppressed tunneling current across their devices. In applying larger source-drain voltages they can observe new excited states forming that result from the edge reconstruction. In contrast, in our capacitance measurements, we basically work at equilibrium and what we observe is effectively the same as what Oosterkamp et al. observe at zero bias. At low source-drain voltages, due to regions of strongly reduced tunneling rates, they observe similar discontinuities in their spectra.

At high electron number and magnetic field these sharp discontinuities evolve into "hidden" electron states. Oosterkamp et al[18], only seem to see two of these abrupt transitions, and they attribute it to the start of the lower density droplet regime. They also attribute this to a state change in the system. On the other hand, we see more than 10 abrupt transitions, likely caused by a phase transition into a lower energy ground state. We attribute these behaviors to a phase transition between different ordered states driven by electron-electron interactions.

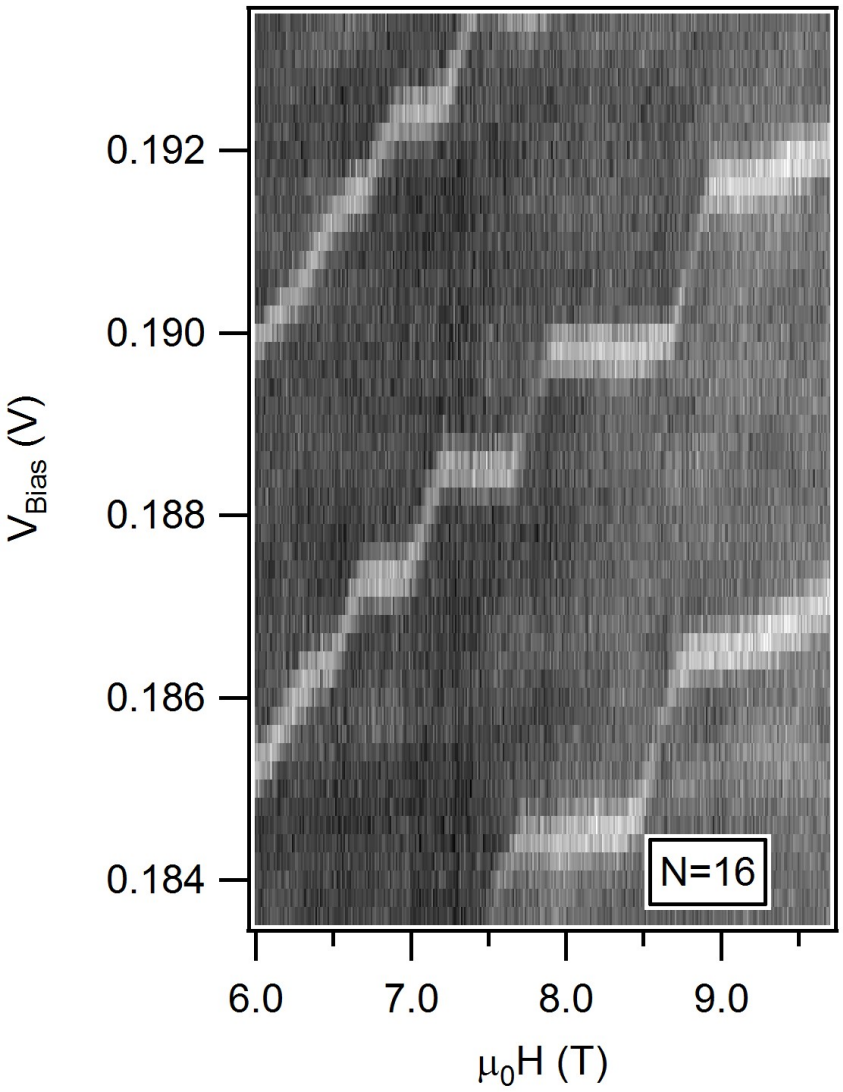


Figure 3-6: Increasing the AC excitations, we can sense the "hidden additions". The AC excitation is $300\,\mu$V.

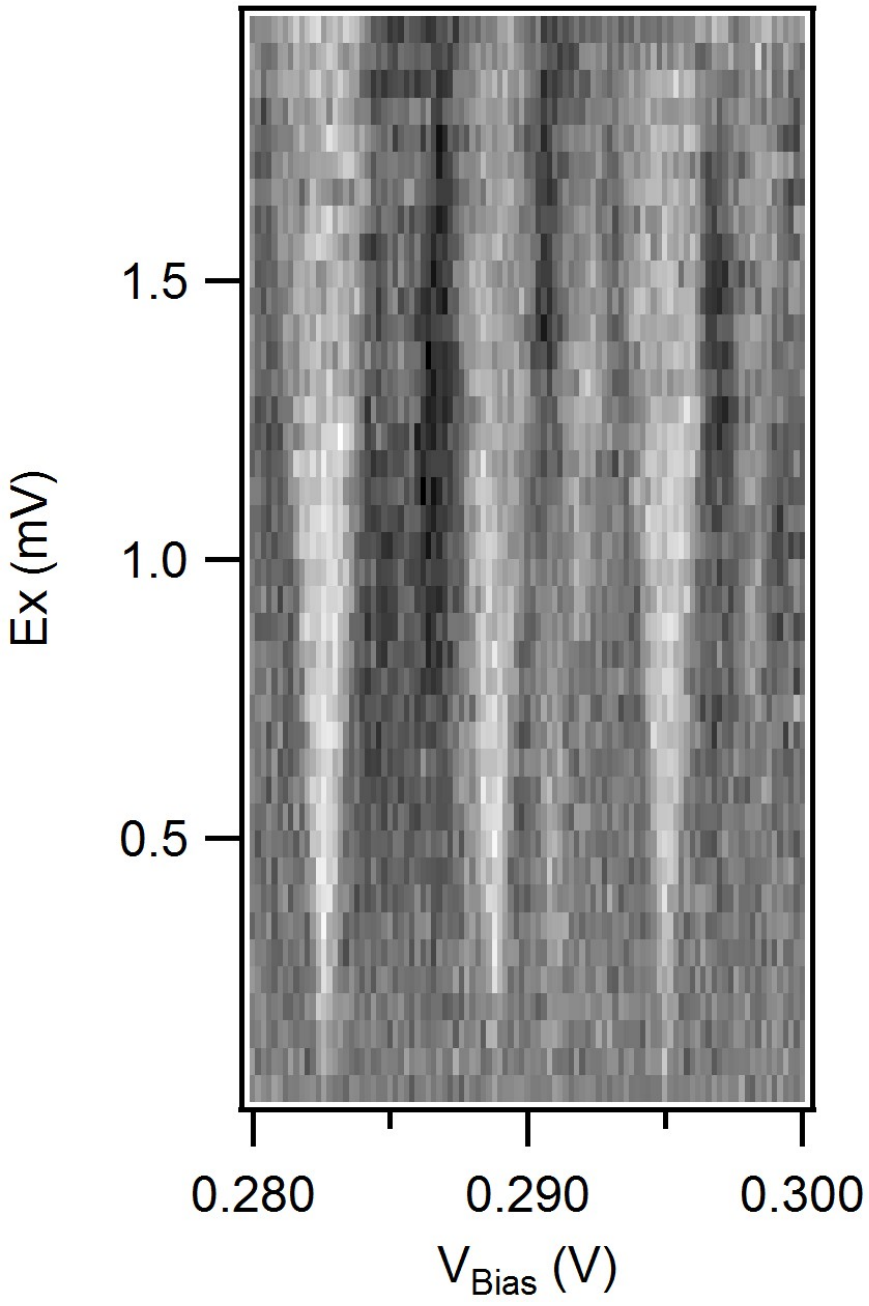


Figure 3-7: The capacitance peak as a function of AC excitations. Electrons appear to be stuck at an energy minimum. At high excitations, electrons have enough energy to overcome this barrier.

THIS PAGE INTENTIONALLY LEFT BLANK

# Chapter 4

# Mini 2DEG

## 4.1 Introduction

Previous studies of electron addition spectroscopy with both vertically and laterally defined quantum dots have focused on relatively small dots. Complementing our study of small quantum dots, we study quantum dots with significantly larger area to explore many electron interactions and the origins of fractional quantum Hall (FQH) states. Most FQH states can be understood as an interaction between single electrons bound to an integer number of quantized vortices within composite fermion theory[4, 37]. Fractions outside of the composite fermion sequence, such as the fraction at filling factor $\nu = 5/2$, must result from more complicated interactions[38]. In particular the $\nu = 5/2$ state has been commonly interpreted as resulting from a condensate of paired composite fermions described by the Pfaffian wavefunction[5, 6], which would exhibit non-Abelian braiding statistics useful for topologically protected quantum computation[39, 40, 41]. Having this in mind, we studied large quantum dots (effectively small 2D electron systems) to understand the underling mechanism responsible for fractional quantum Hall states.

Increasing the sample size by an order of magnitude, we observe effectively quantum Hall physics in comparison to Coulomb blockade physics we have shown in previous chapter. Under the presence of an external magnetic field, electrons in a mini 2DEG develop Landau levels. Here we present capacitance data from a large dot

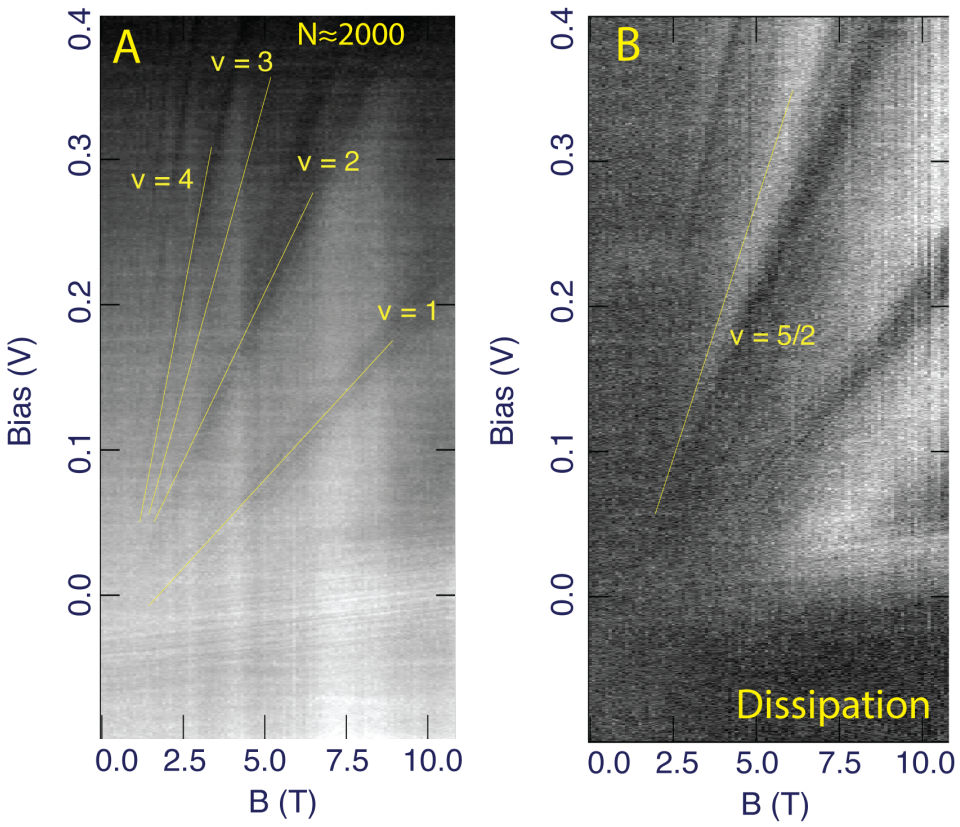


Figure 4-1: (A) Capacitance gaps of a mini 2DEG. Under a perpendicular magnetic field, a 2DEG forms Landau levels. We observe capacitance gaps corresponding to each integer filling factor up to $\nu = 8$. (B) Dissipation plot. In the lighter regions, the dissipation goes higher as the tunneling rate slows down.

of 800 nm lithographic diameter. Figure 4-1 provides a guide for the phase space. Complete gate bias scans are taken at a sequence of fixed magnetic fields. After subtraction of a smooth background, we obtain a two-dimensional array of the sample capacitance as a function of magnetic field and gate bias.

Electrons start to populate the dot at around $V_{BIAS} = -0.1V$. When there are sufficiently many electrons in the dot, we observe the integer quantum Hall states as we sweep the external magnetic field from 0T to 10T. In Figure 4-1A darker regions correspond to fully filled incompressible states whereas lighter regions correspond to partially filled compressible metallic states. The filling factor $\nu$ is the number of spin polarized Landau levels filled with electrons. We control $\nu$ by changing the 2D electron density at a constant magnetic field to fill the Landau levels successively. Alternatively one can maintain the 2D system at a fixed density while changing the magnetic field so that $\nu$ changes due to variation in the degeneracy of the Landau levels.

In Figure 4-1B, we show the dissipation as a function of gate voltage and external magnetic field. When the dot is depopulated, there are no available states to tunnel into. As a result the dissipation is zero below $V_{BIAS} = -0.1V$. We perform our measurements at a frequency (f=247 kHz) well below the zero field roll-off frequency of tunneling barrier(Chapter 2.4). Figure 4-1B shows zero dissipation in the low magnetic field regime. However in high magnetic fields, we observe a slow-down in the tunneling rate which allows us to pick up dissipation. We also observe a surprising enhancement in dissipation along filling factor $\nu = 5/2$ indicating a surpression of tunneling rate.

## 4.2 First Electron Additions to Mini 2DEG

In Figure 4-2, the first electron addition to mini 2DEG appears at $-0.094$ V at zero magnetic field. All peaks start out with nearly zero slope and move monotonically to higher gate bias with increasing magnetic field. At high B fields the curves run nearly parallel to the line $E = \hbar\omega_c/2$, with $\hbar\omega_c$ being the cyclotron frequency. The

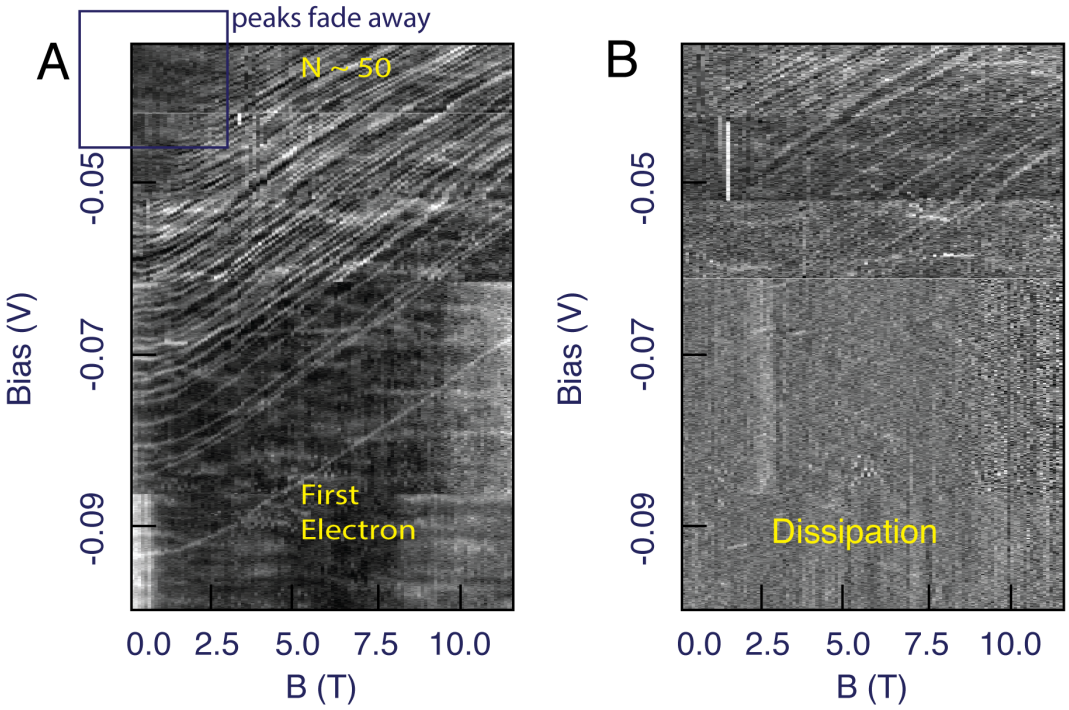


Figure 4-2: (A) Starting from first electrons, the single electron additions to mini 2DEG. As we add more electrons the charging energy decreases. The energy spacing between subsequent electrons also decreases. After the addition of roughly 40 electrons, we are losing the single electron resolution. The horizontal lines are artifact from patching different data sets into one single figure. (B) The very first few electrons enter to the dot with no dissipation. For some electron additions, the a dissipation peak is observed.

data are taken with a small excitation 200 µV at 247 kHz, a frequency sufficiently lower than the tunneling rate so that the electrons can tunnel in and out of the dot in-phase with the applied excitation. As more electrons are added to the dot, the charge droplet expands laterally, and this increases the capacitance of the droplet to the surroundings, thereby decreasing the charging energy for electron additions. Eventually the charging energy diminishes below experimental resolution, and the capacitance peaks slowly diminish as in the top left region in Figure 4-2.

## 4.3 Localized States

In the absence of disorder, Landau levels occur at sharply defined intervals of the cyclotron energy $\hbar\omega_c$ as in Figure 4-3A. Disorder due to defects and impurities leads to localization of electron wavefunctions in the sample and the broadening of Landau levels. In the single-particle picture, electrons populate states in a fixed disorder potential. However, Coulomb repulsion produces a potential landscape that varies with the filling factor in an attempt to minimize the total electrostatic energy[42]. The capacity of screening the disorder potential is maximized when the Fermi energy is tuned to partially filled landau level. In between Landau levels as in Figure 4-3B, there is less screening of the electrons due to lower density of states within a Landau gap. In Figure 4-4, we show two distinct groups of interaction driven localized states that appear at filling factors $\nu = 1$ and $\nu = 2$. Those localized states follow the slope of the underlying Landau levels and appear only when the landau level is fully filled. Screening of the electrostatic potential arising from disorder depends sensitively on Landau level filling factor[42, 43, 10]; a partially filled significantly screens the disorder potential but, around integer $\nu$, the electronic density of states is small and the disorder potential is poorly screened, leading to compressible charge pockets separated by incompressible barriers. In Figure 4-4, the peaks that run parallel to integer $\nu$ arise from electron additions to these pockets[44, 45, 46].

Similar peaks appear around every well-developed integer quantum Hall state as also appeared in previous work[44] studying a 2DES gated by a local scanning single electron transistor (SET)[44, 47, 48]. The charging peaks in that prior work arose from electrons moving laterally within a very large 2DES to fill individual localized compressible islands in an otherwise incompressible region. In contrast, charge quantization always occurs in our lithographically defined quantum dots, allowing us to observe single electron additions into both compressible and incompressible regimes. This capability has led us to observe a remarkable series of periodic electron additions that appear in the compressible regions.

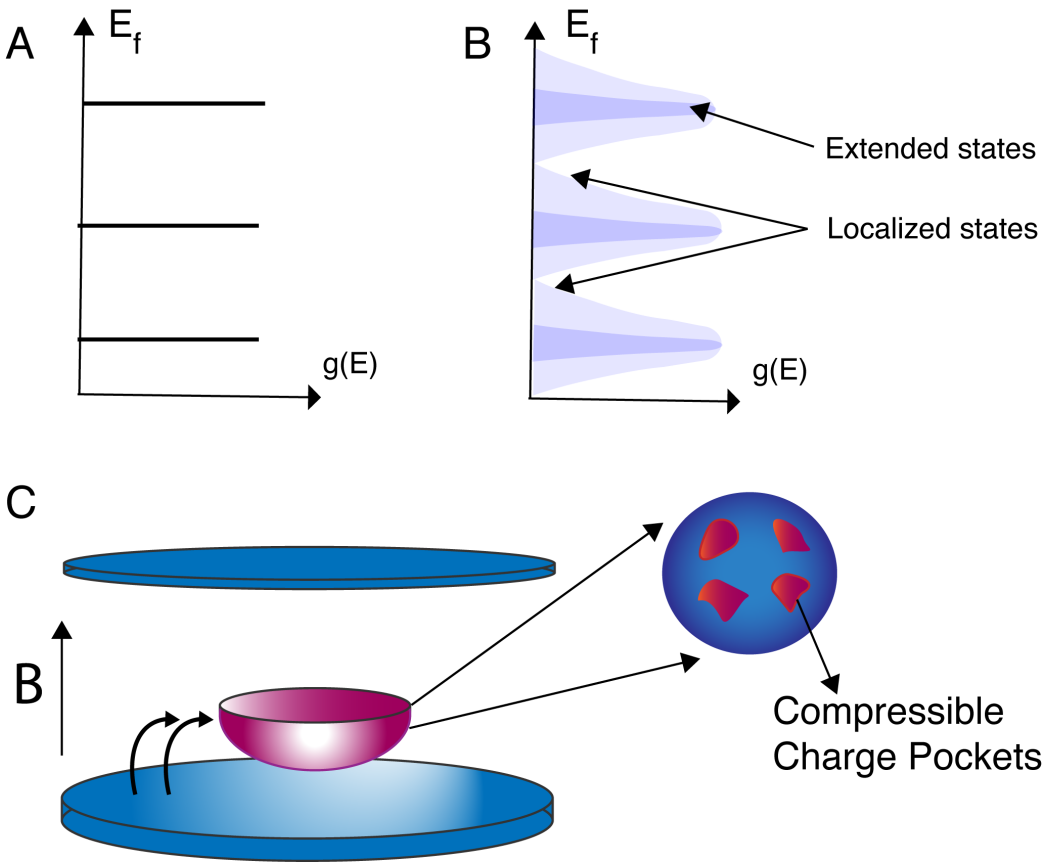


Figure 4-3: (A) Landau levels of a 2DEG in a clean and (B) in a disordered sample. Disorder due to defects and impurities leads to localization of electron wavefunctions in the sample and the broadening of Landau levels. (C)The compressible charge pockets are surrounded by an incompressible barrier.

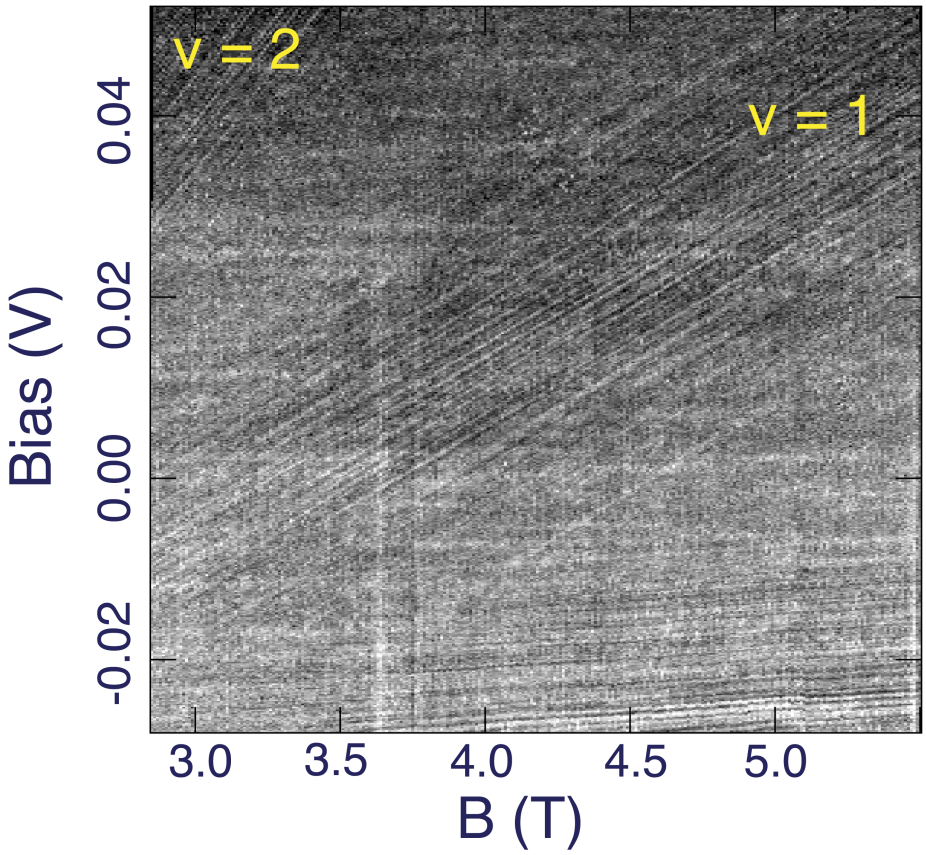


Figure 4-4: Localized states within the incompressible regions. These states, unlike the extended states in the bulk, are confined to a small region within the gap. Therefore, they follow the underlying filling factor. Here we present the localized states within filling factor $\nu = 1$ and $\nu = 2$. The states that are nearly parallel to field axis are the first electrons.

THIS PAGE INTENTIONALLY LEFT BLANK

# Chapter 5

# Pairing of Single Electron Additions at the Edge

## 5.1 Introduction

We now focus on performing fine measurements at compressible and regions with very large numbers ($\sim 2000$) electrons in the dot. In Figure 5-1, we observe unpredicted states that are evenly spaced in magnetic field. Unlike the electron additions in a small quantum dot (Fig 1c) where the electron addition peaks show zig-zags, the spectra show only uniform straight lines. The energies of these states all move down with increasing magnetic field, as would be expected only for electronic states at the edge of the mini-2DES.[20] To our surprise, we do not see any sign of states moving up in energy. This observed downward movement of all observed states and the perfect periodicity suggest that the edge of the 2DES remains "compact", with all angular momentum states filled. This is the situation that is sometimes expected at filling factor $\nu = 1$[49, 18] in a "maximum density droplet" (MDD) with no "edge state reconstructions"[50] occuring in the range of these data sets. In the case of such a $\nu = 1$ MDD, one would expect a single electron addition for each additional magnetic flux quantum ($h/e$ of magnetic flux) threaded through the dot. We note that our data at these densities and filling factors do not always display all electron additions to the dot. In a large area 2D electron system, tunneling from a 3D electrode into the bulk

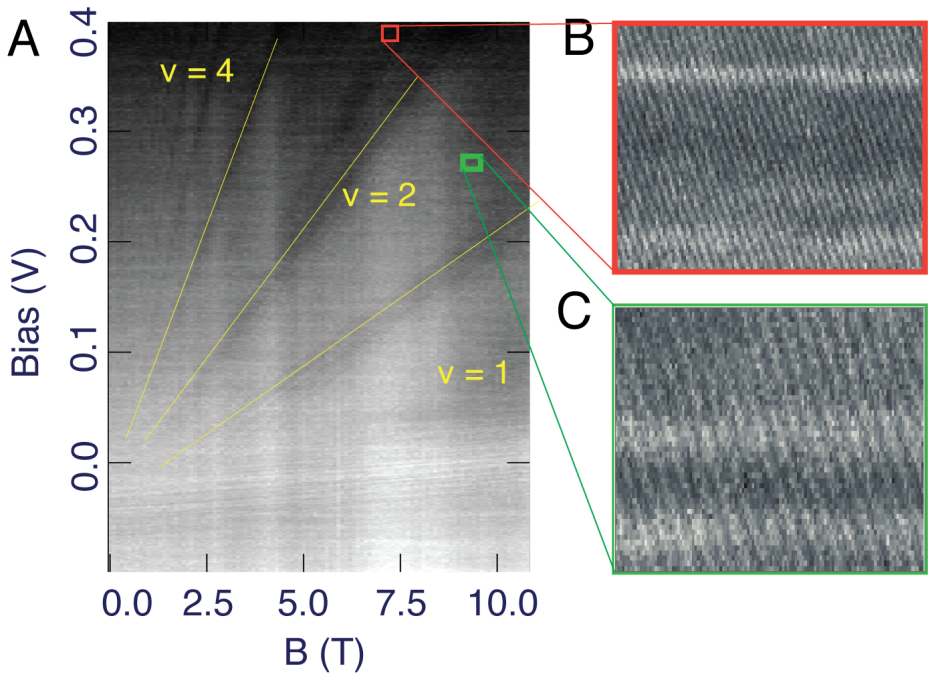


Figure 5-1: (A) Capacitance plot of mini 2DEG as a guide for the phase space. (B) Between filling factors $\nu = 2$ and $\nu = 5$, we observe, almost exclusively, states that move down in energy with magnetic field, as expected for edge states. (C) Between filling factors $\nu = 1$ and $\nu = 2$, these appear periodically in magnetic field with a period that corresponds to a flux quantum of h/e treading the dot. However, between filling factors $\nu = 2$ and $\nu = 5$, the field periodicity of the peaks halves resulting h/2e oscillations.

of 2D system is suppressed exponentially by a magnetic field induced Coulomb gap to tunneling[51]. In contrast, there is only power-law suppression for tunneling into edge states[52], and electrons tunneling to the edge still do so at short time scales compared with the inverse frequencies of the ac excitations in our measurements. At fixed gate bias, electrons enter the dot as we increase magnetic field, but charge balance can be maintained as electrons, not visible to the experiment(due to low tunneling rate), tunnel out of the dot from the dot-center to the tunneling electrode.

In the following chapters, we present data taken on two QDs, one of which is twice as large as the other. Most of the data presented is from the larger one unless it is explicitly stated.

## 5.2 Isolated Tunneling to Edge States

This observed downward movement of all observed states and the regular periodicity observation suggest that the dot remains compact, as would be expected in a "maximum density droplet" with no "edge state reconstructions" occuring in the range of these data sets. During a tunneling event, the small excitation signal (200 µV RMS) we apply only results in observable peaks from the edge states despite the fact that the bulk is partially filled.

At the edges of the 2DEG, the electron density changes from zero at the edge to its bulk value through the smooth edge potential in GaAs heterostructure. In previous theoretical works[43, 53], it has been shown that the self-consistent electrostatic potential changes in a steplike manner due to the formation of alternating stripes of compressible and incompressible electron liquids. In Figure 5-2 we visualize this step like edge potential and resulting compressible edge state and the incompressible stripe between the edge and the bulk while the filling factor is between $\nu = 1$ and $\nu = 2$. In figure 5-2, being inspired from Chklovskii's work[43, 53], we show how the single particle picture differs from self-consistent electrostatic picture resulting in stripes of incompressible regions between the edge and the bulk.

Consistently, in the capacitance measurements, we can detect the single electron additions to edge states mainly at high densities and high magnetic fields. Keeping the density constant, we observe that the bulk-edge separation is strongest between filling factor $\nu = 2$ and $\nu = 3$. As we reduce the magnetic field(moving to higher filling factors), the capacitance signal that comes from the tunneling to edge states gets weaker but it is still visible until the filling factor $\nu = 5$. However in the low magnetic field region, we cease to observe isolated edge states.

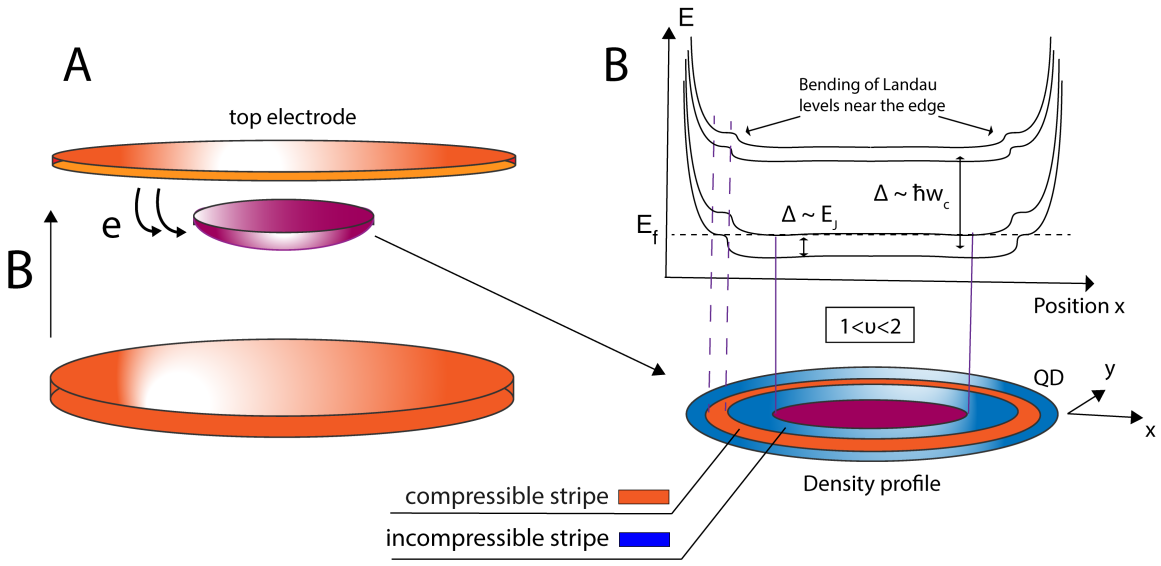


Figure 5-2: Quantum Hall edge states profile. (A) Vertical capacitance structure under external magnetic field. (B) The energy profile when the density is tuned to between filling factor $\nu = 1$ and $\nu = 2$. Due to the increasing potential near the edge, we observe the bending Landau levels. The edge channel has a finite width. Below that we show the electron density as a function of the distance to the boundary. Red strip represent regions with compressible liquid, blue strip represent incompressible liquid.

## 5.3 2e Electron Charge Tunneling

Testing the possibility of electron pairing in the tunneling event, the amount of charge transferred is determined using the capacitance height. This indeed showed 2e charge being tunneled back and forth between the electrode and QD.

Contrary to the belief that it would take more energy to add each successive electron to a quantum dot as the electrons would repel each other, our measurements have revealed an astonishing phenomenon: for the high-density regime, electron additions can occur in pairs. In capacitance measurements, we can detect how much charge is tunneled by looking at the peak height[27]. In Figure 5-3, compared to first electrons and the edge states between filling factor $\nu = 1$ and $\nu = 2$, we show that 2e charge is tunneling back and forth to quantum dot when the density is tuned between filling factor $\nu = 2$ and $\nu = 5$. One could argue that the doubling of frequency arises from the fact that there are two edge states between $\nu = 2$ and $\nu = 3$. However, the doubling of peak frequency commences $\nu = 2$ and persists all the way to $\nu = 5$.

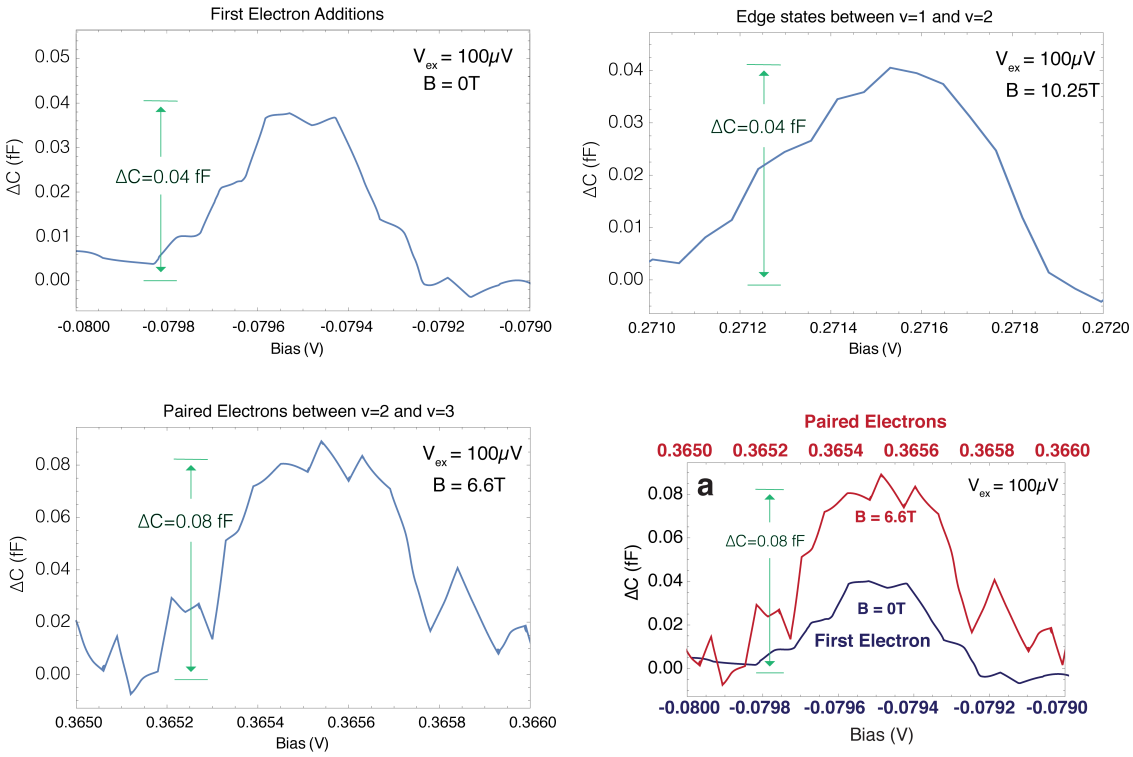


Figure 5-3: Electron charge comparison between one of the first electrons and one of the edge states. The capacitance peak is proportional to $A_v \frac{e^*}{C_{shunt}}$ where $e^*$ is the charge of tunneled electron, $A_v$ is the total gain of the amplifiers, and $C_{shunt}$ is the shunt capacitance to the ground. We show that between filling factor $\nu = 3$ and $\nu = 3$, 2e charge is tunneling back and forth.

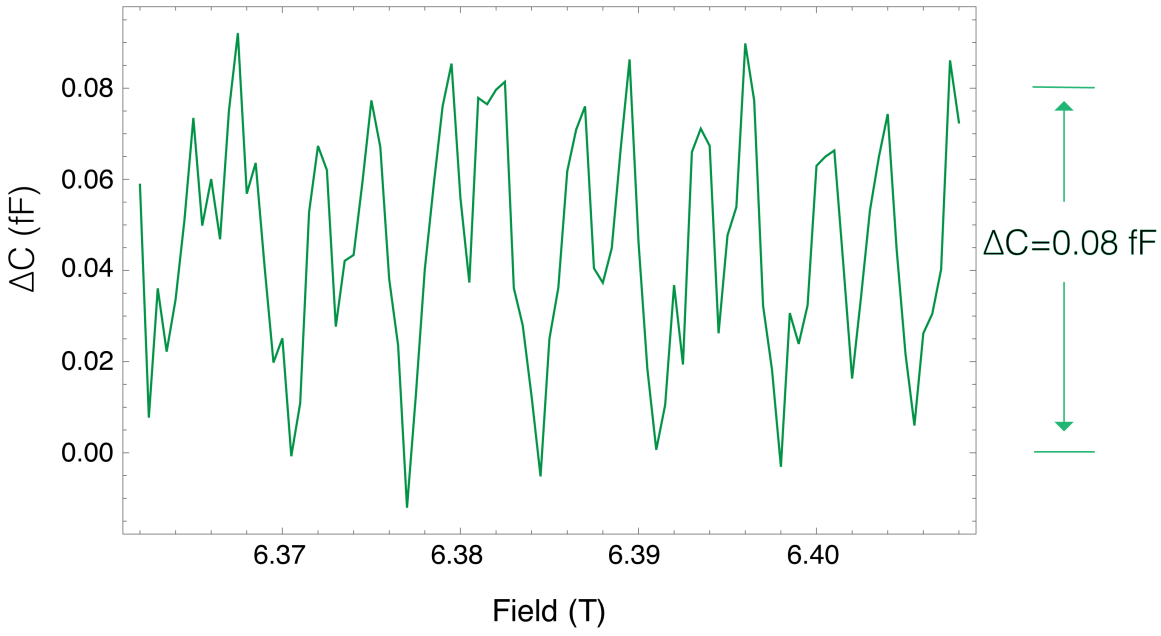


Figure 5-4: Capacitance peaks that correspond to paired electrons as a function of magnetic field. The peak height is directly proportional to electron charge.

## 5.4 Fourier Analysis

To investigate the B dependence of capacitance peaks at constant density, we perform discreet Fourier transformation. Between filling factor $\nu = 1$ and $\nu = 2$, Figure 5-5 shows the capacitance peaks appear periodically in magnetic field with a period that corresponds to a flux quantum of h/e treading the dot. Fourier transform(Figure 5-5C) shows that the periodicity in magnetic field when the filling factor is between $\nu = 1$ and $\nu = 2$ is $\Delta B = 7.4\,\mathrm{mT}$. Consequently, an area of $A = h/e\Delta B = 0.56\,\mu\mathrm{m}^2$ is deduced from $\Delta B$ period. This area is compatible with the lithographic size.

These observations were found to be robust and reproducible in different QDs of different sizes. In a smaller dot, between $\nu = 1$ and $\nu = 2$, we observed that capacitance peaks have field periodicity of $\Delta B = 12.8\,\mathrm{mT}$ indicating an area of $0.325\,\mu\mathrm{m}^2$.

However, between filling factor $\nu = 2$ and $\nu = 5$, the field periodicity of the peaks halves resulting h/2e oscillations. This is clearly evident in the edge states plot near filling factor $\nu = 5/2$. The red curve in Figure 5-6C, shows that the Fourier transform has a frequency peak twice as large indicating multiple windings.

Using the Fourier transform, we can also estimate the capacitance peak height. In this analysis we use the discrete Fourier transform of a sequence of N numbers as:

$$X_k = \frac{1}{N}\sum_{j=1}^{N} x_j \cdot e^{-\frac{2\pi i}{N}kj}, \tag{5.1}$$

where $x_j$ is the $j$th component of the sequence. Assume the sequence $x_j$ has the sinusoidal form , $x_j = Ae^{\frac{2\pi i}{N}\bar{k}j}$, with frequency $\bar{k}$. Then the Fourier sequence will have peak at $\bar{k}$ with an amplitude proportional to $A$.

$$\begin{aligned} X_k &= \frac{1}{N}\sum_{j=1}^{N} Ae^{\frac{2\pi i}{N}\bar{k}j} \cdot e^{-\frac{2\pi i}{N}kj} \\ &= \frac{1}{N}\sum_{j=1}^{N} A \cdot e^{\frac{2\pi i}{N}(\bar{k}-k)j}. \end{aligned} \tag{5.2}$$

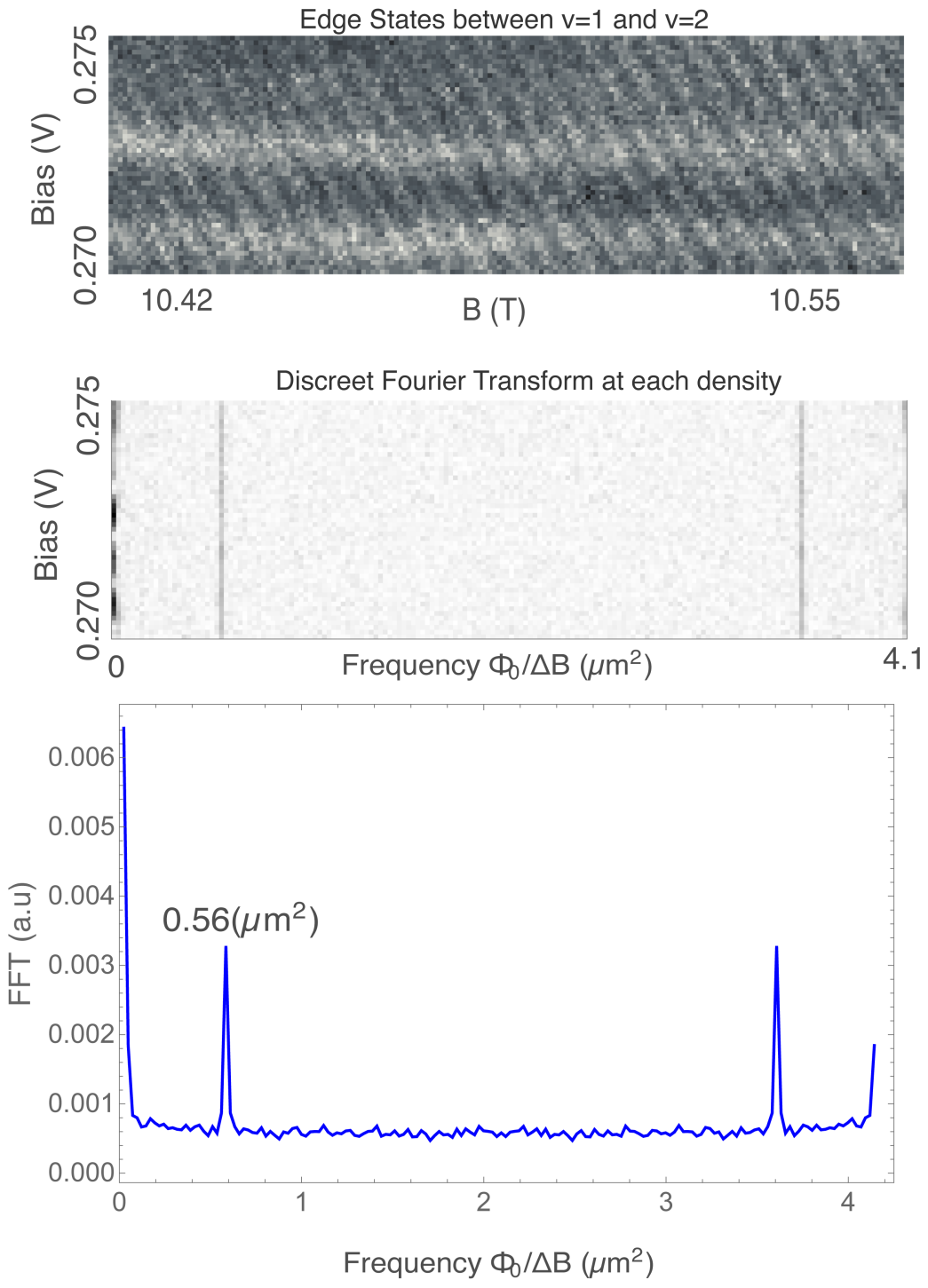


Figure 5-5: (A)Capacitance peaks in the compressible region between filling factor $\nu = 1$ and $\nu = 2$. (B) The discreet Fourier transform of field sweeps at each density. (C) The mean Fourier transform indicating the frequency of the single electron peaks.

In the limit $N \to \infty$ this sum is non-zero only when $k = \bar{k}$ yielding $X_{\bar{k}} = A$. In other words, the height of Fourier component is linearly proportional to capacitance height. We can utilize this to investigate electron height when the data is noisy and we have hard time isolating a single peak. In this analysis we have taken account the different point spacing and different record lengths.

In Chapter 2.6, we have demonstrated the expected response of electron tunneling as a function of excitation voltage. For $v_{rms} \gg \eta k_B T/e$, the peak height saturates $\propto \frac{e}{C_{shunt}}$, and the base width broadens twice the amplitude of the AC excitation. Since we ran the measurements with an excitation voltage $v_{rms} = 200\,\mu$V much higher than $k_B T/e$, we expect the capacitance height to be saturated and be proportional to electron charge.

In Figure 5-6C, we observe that the Fourier component near filling factor $\nu = 5/2$ is twice as large as near filling factor $\nu = 3/2$. Since we have run the measurements in the same cool down, with the same operation point, with the same total shunt capacitance; this observation suggests that the capacitance peak height (correspondingly the quantized electron charge) near filling factor $\nu = 5/2$ is twice as large as near filling factor $\nu = 3/2$. However this Fourier analysis isn't our main basis for concluding the 2e charge tunneling. In Chapter 5.3, we have argued our reasoning.

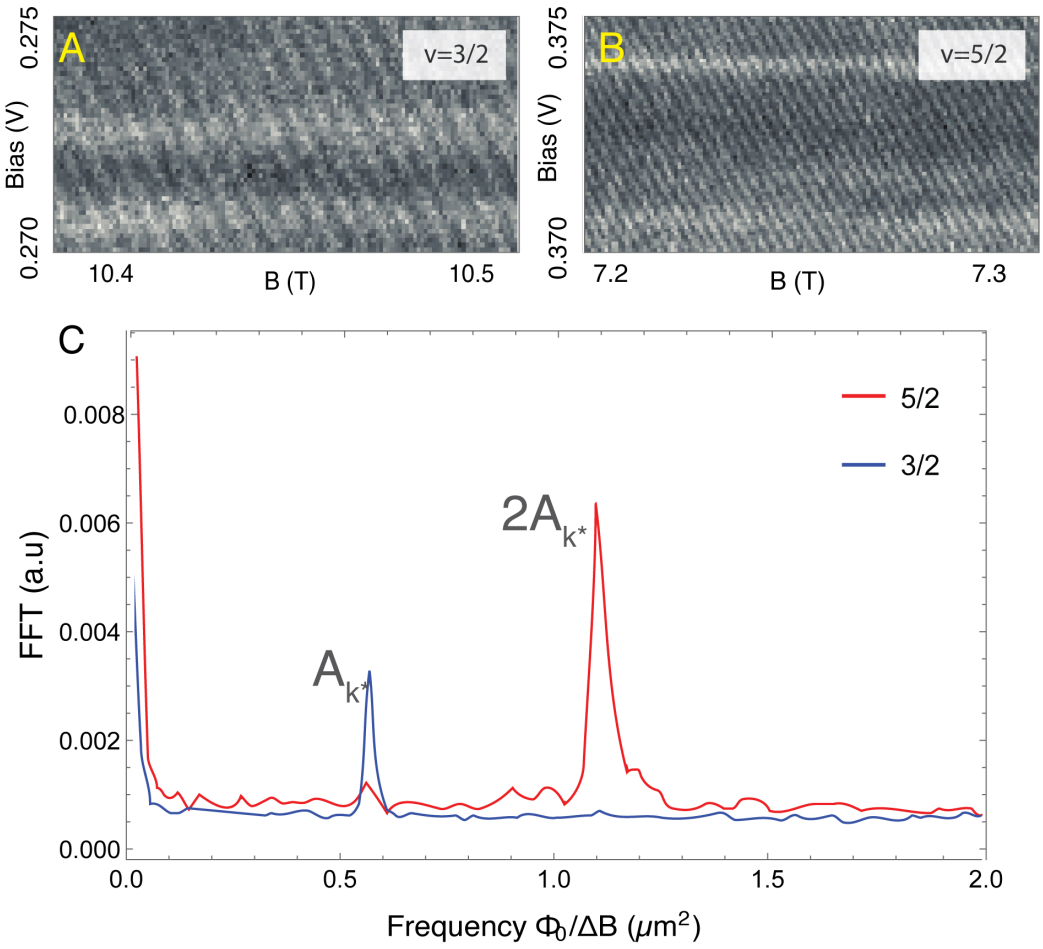


Figure 5-6: Capacitance peaks at h/e and h/2e. (A) Capacitance data taken as a function of gate voltage and magnetic field in the h/e regime. The filling factor is near $\nu = 3/2$. (B) When the gate voltage is tuned to near filling factor $\nu = 5/2$, the periodicity in magnetic field is halved. (C) Corresponding Fourier transforms of two different regions as a function of $\Phi/\Delta B$. Blue curve is the Fourier transform near $\nu = 3/2$, and the red curve is for near $\nu = 5/2$ indicating a Fourier peak at an area twice as large as the peak for the blue curve.

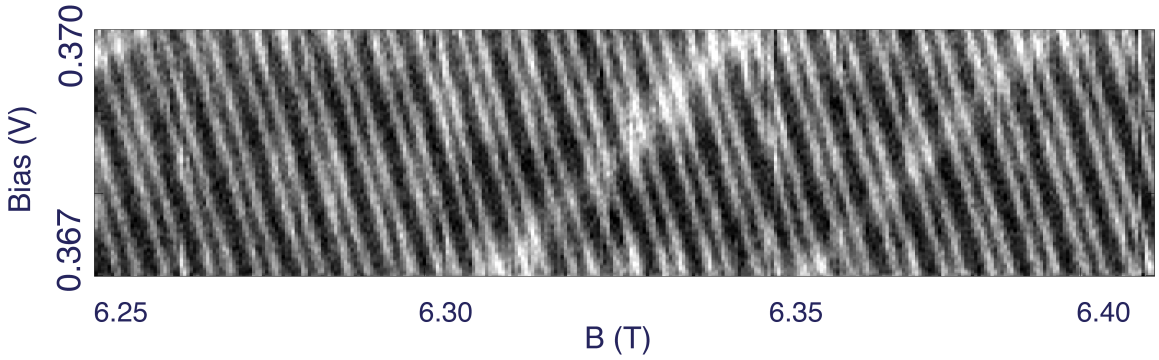


Figure 5-7: A very fine measurement is performed to narrow down the peaks even more. The AC excitation is 100 µV. We also see the localized states non-interacting with the edge states at all.

## 5.5 Bunching Phenomena

What is even more surprising to us is the observation of bunching phenomena between $\nu = 2$ to $\nu = 5$. In Figure 5-7, we are presenting our finest data taken with 100 µV excitation voltage with sub-milliTesla field steps. The main result from this experiment is that the 2e electron peaks come also in pairs.

Figure 5-8 shows this bunching behavior while sweeping magnetic field from $\nu = 2$ to $\nu = 3$. As it is depicted in Figure 5-8, we concluded that bunching occurs for all compressible filling factors between $\nu = 2$ and $\nu = 3$ except for a narrow region around $\nu = 5/2$. The bunching phenomena continue showing up until the filling factor $\nu = 5$. The halving of periodicity, bunching phenomena, and localized states have been observed in another sample which has an area of 0.325 µm$^2$ as well.

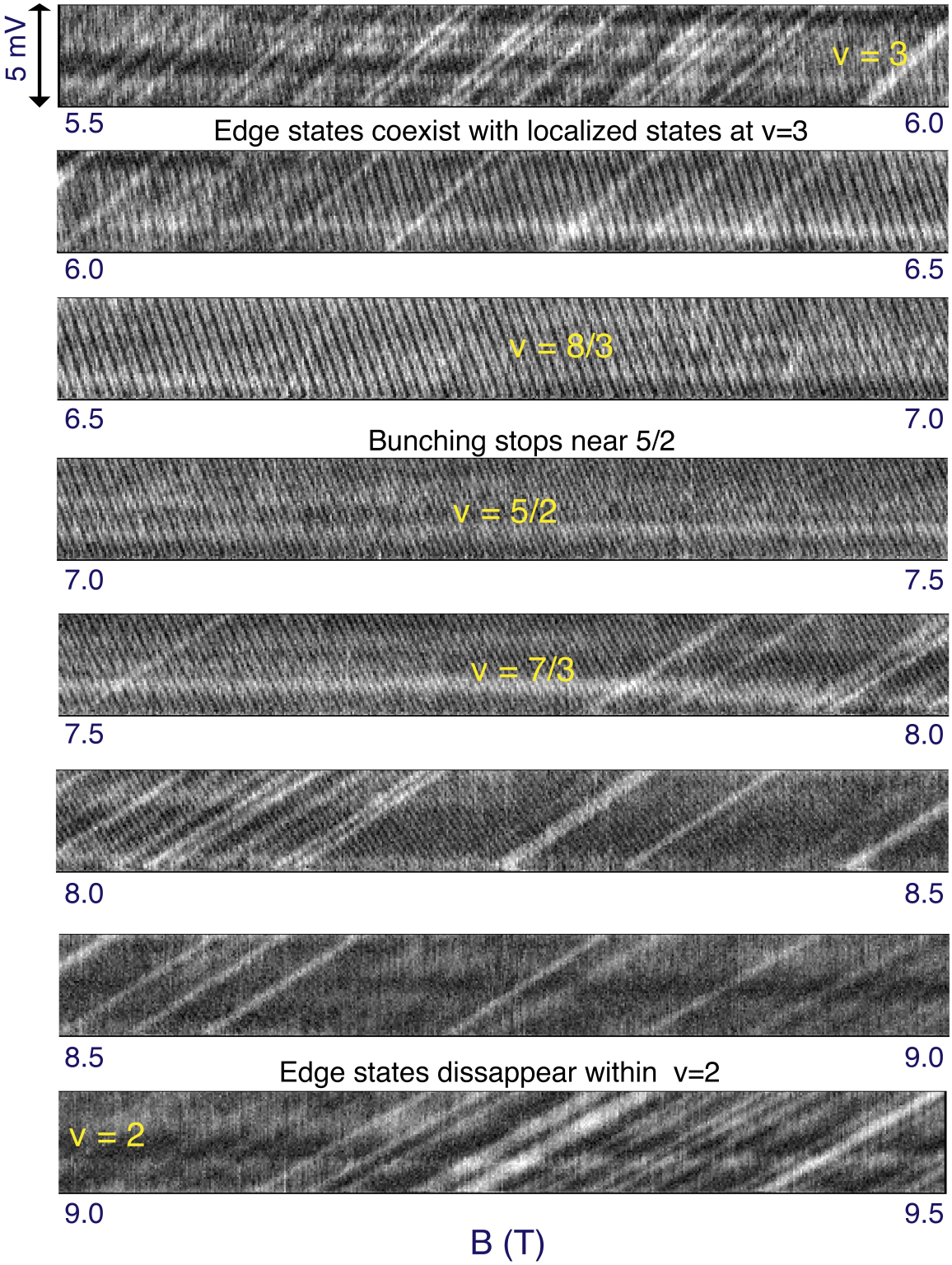


Figure 5-8: Edge states between $\nu = 2$ and $\nu = 3$.

The ranges of filling factors over which we observe the pairs and their occurance in edge states, suggests a close relation to observed pairing of electrons seen in an entirely different type of experiment[1, 54] utilizing an electronic version of Fabry-Perot interferometer(FPI)[55]. The FPIs are fabricated on a 2DEG confined by two quantum point contacts. Allowing only the outermost edge through the QPCs, FPI is predicted to have conductance oscillations when the total flux is changed by one flux quanta(h/e). This predicted behavior has been observed between filling factors $\nu = 1{-}2$, however the periodicity in magnetic field is halved, yielding h/2e oscillations, at a wide range between filling factor $\nu = 5/2$ and $\nu = 5$. In addition, the quantum shot noise measurements at QPC yield a quasiparticle charge equal to the electron charge at filling factor $\nu = 1$ and $\nu = 2$, whereas the quasiparticle charge is twice the electron charge at filling factor from $\nu = 5/2$ to $\nu = 5$. These observations suggest that the pairing exists within one interfering edge channel though the exact mechanism causing edge state attraction is still unknown.

These observations are compatible with our results despite the experiments are substantially different. In capacitance measurements on quantum dots, we see capacitance peaks corresponding to single electron tunneling to edge states whereas FPI interferometer shows the conductance oscillations. In Figure 5-7, we can isolate each electron peak by increasing the averaging time after narrowing down the peak width. This is a simple evidence that our peaks are not some sort of sinusoidal oscillations but dirac delta functions broadened by temperature and AC excitation.

**To summarize,**

- The h/e oscillations between filling factors $\nu = 1 - 2$ are in perfect agreement in both experiments.
- The h/2e periodicity appears between $\nu = 2$ and $\nu = 5$ in quantum dot measurements whereas it appears between $\nu = 5/2$ and $\nu = 5$ in FPI measurements.
- Capacitance measurements show single electron transitions whereas FPI measurements show conductance oscillations.

- Capacitance peaks have 2e charge between $\nu = 2$ and $\nu = 5$, the shot noise at FPI's quantum point contact indicates 2e electron charge between $\nu = 5/2$ and $\nu = 5$.

- Capacitance measurements show 2e charged peaks pair up between $\nu = 2$ and $\nu = 5$ except for filling factor $\nu = 5/2$. Bunching of the capacitance peaks have no correspondence in FPI measurements.

Having two entirely different experiments showing similar results is intriguing in the sense that the underlying mechanism might be the same. Capacitance measurements show a periodicity that corresponds to h/2e oscillations between filling factor $\nu = 2$ and $\nu = 5$, and the electron additions bunch in pairs in this range except for a the vicinity of $\nu = 5/2$ where bunching disappears for a very narrow range.

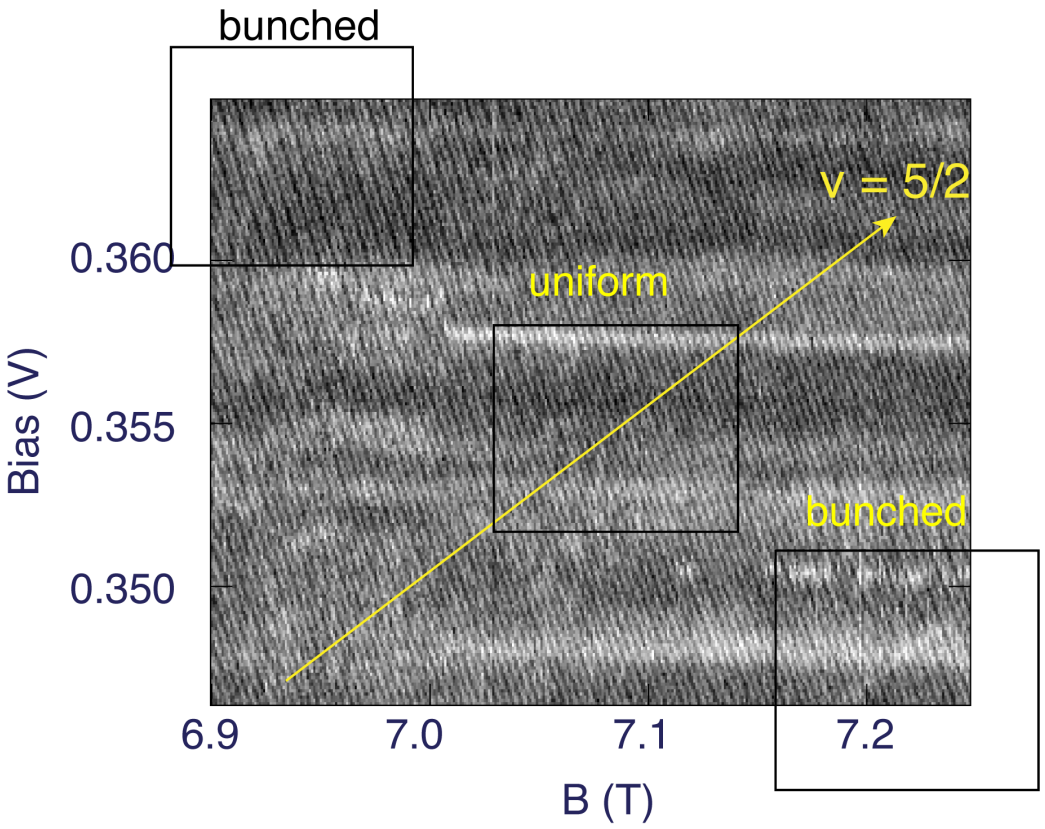


Figure 5-9: We observe that edge states bunch everywhere between $\nu = 2$ and $\nu = 5$, except for the narrow band at $\nu = 5/2$. This figure illustrates how the bunching transitions to uniform peaks.

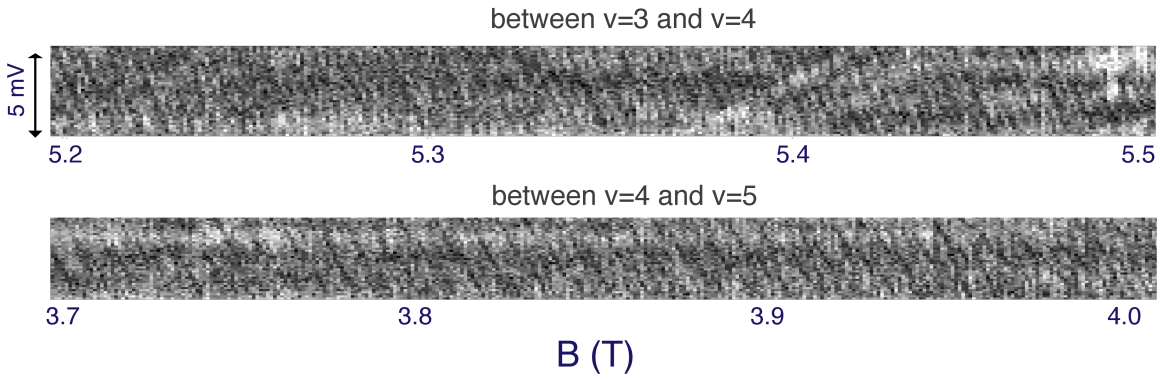


Figure 5-10: We observe that edge states between $\nu = 3$ and $\nu = 4$ as well as between $\nu = 4$ and $\nu = 5$.

### 5.5.1 Beyond filling factor $\nu = 3$

The pairing appears between filling factor $\nu = 3$ and $\nu = 5$ except when the density is tuned into around integer filling factors. Within the gaps, we lose resolution of the edge states mainly because of dominance of the localized states. In Figure 5-10, we show the capacitance peaks in two different compressible regions. Fourier analysis revelas that for filling factor $\nu > 3$, we have the same magnetic field periodicity as the pairing between $\nu = 2$ and $\nu = 3$. This rules out the simple argument in which the number of available edge states determine the magnetic field periodicity. One might naively expect that, for instance, between $\nu = 3$ and $\nu = 4$, we have three edge states indicating $h/3e$ oscillations, but this is not what we observe.

## 5.6 Missing Bulk States

In this section, we present arguments to account for the missing bulk states. Along the magnetic field direction while the gate voltage is constant, electrostatics considerations suggest that the number of electrons in the dot should remain roughly constant. At fixed gate voltage, as we increase the magnetic field, we, instead observe periodic electron additions to the edge, seemingly suggesting an increase in the number of electrons within the dot. However, at constant gate voltage, the electrostatics makes it implausible to keep adding electrons along a wide range of magnetic field.

We resolve this conundrum by noting that, due to significant tunneling suppression to the bulk[30], the bulk states may become invisible to our measurements. Since quantum Hall edge states have similar low energy excitations as Luttinger liquid[56, 57], their tunneling behaviour has power-law temperature dependence[52] whereas tunneling to the bulk has exponential dependence. Consequently, the small AC excitation we use in capacitance measurements is only capable of sensing the edge states.

We estimate the total number of electrons added to the quantum dot to completely fill a spin polarized landau level. At a specific field value($B = 7.2\,\mathrm{T}$), that number is given as $BA/\Phi_0$. At the same magnetic field, between filling factor and $\nu = 2$ to $\nu = 3$, we estimate the number of electrons added to the edge by counting the number of capacitance peaks. Comparing those two numbers, we show that there are more electron additions to the QD than the number of electrons added to the edge. In other words, as we sweep the gate voltage, we add electrons both to the edge and also to the bulk. Our measurement is only capable of sensing the edge states due to tunneling suppression to the bulk.

Here we show how we performed this analysis. Figure 5-11 shows data from the edge states between filling factors $\nu = 2$ to $\nu = 3$ at a narrow field range around B=7.2T. Between the centers of filling factor $\nu = 2$ and $\nu = 3$, we count total 239 peaks. Since we know each peak holds 2 electrons, this makes $N_{edge} = 478$ electrons. From the periodicity of field oscillations(h/e), we deduce the area of this sample to

be $0.56\,\mu m^2$. Given this area, at magnetic field B=7.2 T, we expect the Landau level to have a degeneracy of,

$$N_\Phi = \frac{B.A}{h/e} = \frac{(7.2\,\mathrm{T})(0.56\,\mu m^2)}{4.13\,\mathrm{mT}\mu m^2} = 976$$

$$N_\Phi \approx 2N_{edge}$$

This discrepancy tells us that we are electro-statically adding $N_\Phi$ electrons, and observing only some of those electrons as edge states. The ratio of the number of electrons added to the bulk vs to the edge is sample dependent. Depending on the area of the bulk against the edge, this ratio might be different.

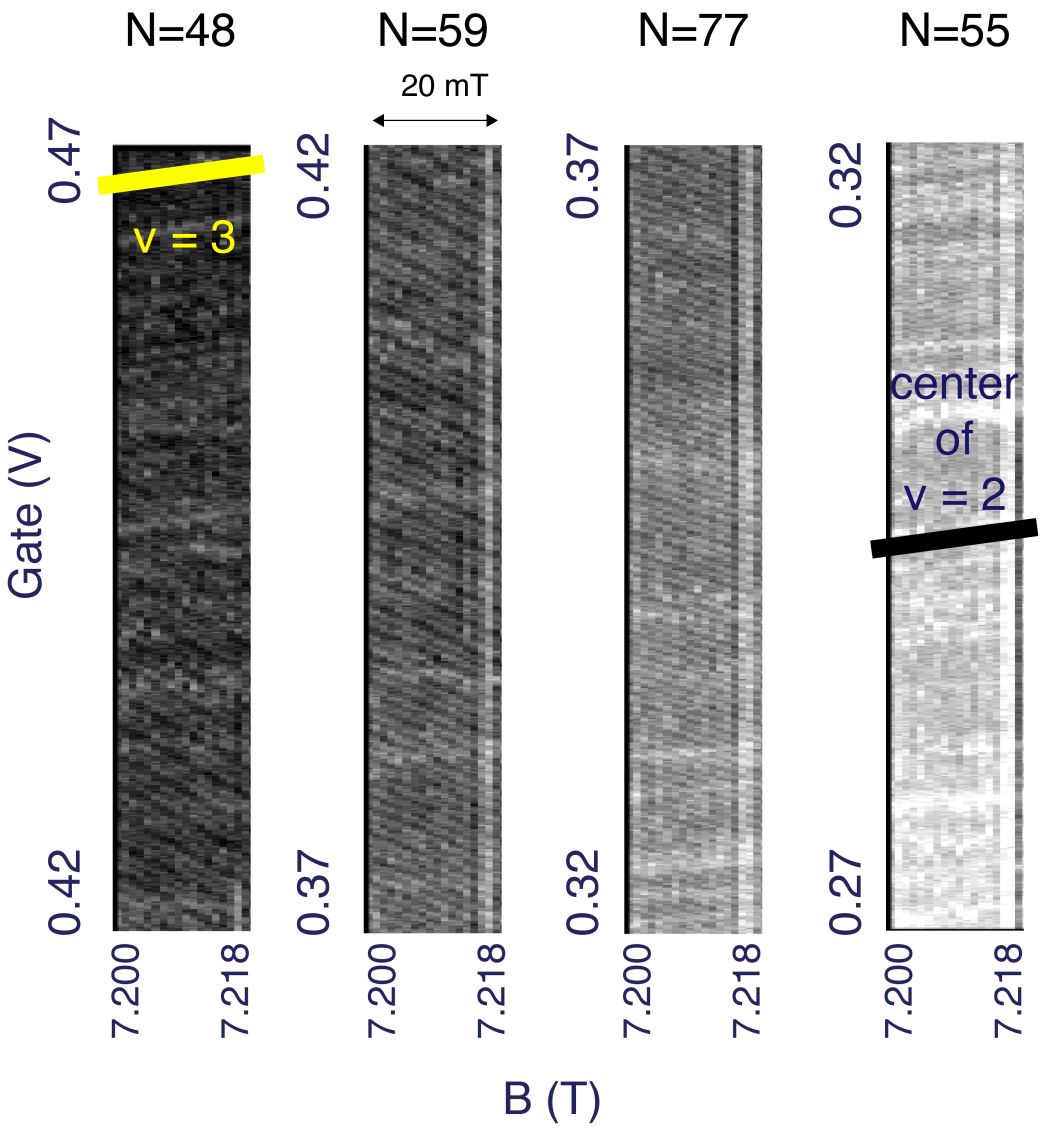


Figure 5-11: Edge states from filling factor $\nu = 2$ to $\nu = 3$ at a narrow field range around B=7.2T. To make the edge states visible to the eye, the plot is cut into four pieces. Between the center of filling factor $\nu = 2$ and $\nu = 3$, we count total 239 peaks.

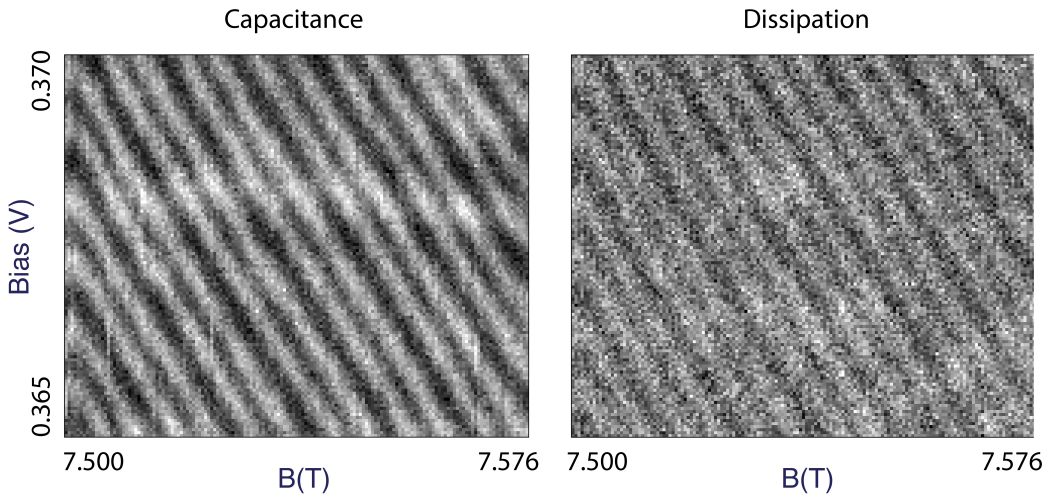


Figure 5-12: Capacitance and dissipation data for edge states between filling factor $\nu = 2$ to $\nu = 3$. The excitation voltage is $V_{exc} = 150\,\mu\text{V}$. The area for this sample is $A = 0.325\,\mu\text{m}^2$.

In Figure 5-12, we present capacitance and dissipation data for some edge states. Observing high dissipation means that the electron tunneling slowed down as compared to measurement frequency $f = 247\,\text{kHz}$.

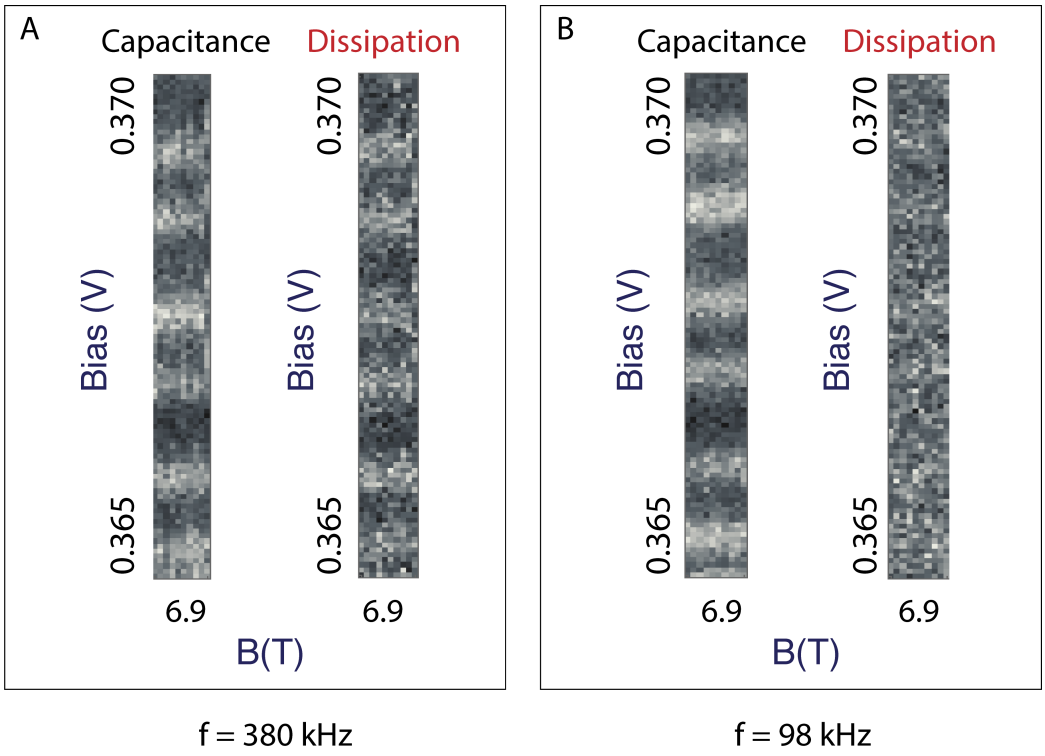


Figure 5-13: Dissipation at two different frequencies, (A)$f = 380\,\text{kHz}$ and (B) $f = 98\,\text{kHz}$. The dissipation disappears at $f = 98\,\text{kHz}$ while we still see the edge states in the capacitance at this frequency. The magnetic field is fixed at $B = 6.9\,\text{T}$. The excitation voltage is $V_{exc} = 100\,\mu\text{V}$. The area for this sample is $A = 0.56\,\mu\text{m}^2$.

THIS PAGE INTENTIONALLY LEFT BLANK

# Chapter 6

# Fabrication of Quantum Dots

In this section, we describe the process for fabricating our quantum dots. The goal of this fabrication process is to confine electrons in small pockets within the quantum well plane, and to make contacts to the top and the bottom electrodes of the tunnel capacitor. Creating submicron quantum dots and detecting single electrons in capacitance measurements require us to reduce the shunt capacitance as much as possible. Therefore, we define a mesa, make deep ohmic contact to the bottom electrode, define dots, lay out metal on the dots, and finally make contacts to the dots. The detailed fabrication process is listed in Appendix A.

The AlGaAs/GaAs wafer contains the following layers in Table 6. Fabricating very small dots can be very challenging due to large thickness of the conducting mesa. To increase the yield of small sized quantum dots, we reduced the thickness of top contact electrode quite dramatically.

| | | | |
|---|---|---|---|
| | substrate | GaAs (undoped) | |
| 1 | bottom initial growth | GaAs(intrinsic) | 3000 Å |
| 2 | bottom blocking barrier | $Al_{0.323}Ga_{0.677}As$ | 4000 Å |
| 3 | bottom electrode | GaAs(n+, $4 \times 10^{18}$) | 2000 Å |
| 4 | bottom electrode | GaAs(n+, $1 \times 10^{18}$) | 1000 Å |
| 5 | bottom spacer #1 | GaAs(intrinsic) | 30 Å |
| 6 | **cold growth/diffusion barrier*** | GaAs(intrinsic) | 30 Å |
| 7 | blocking barrier | $Al_{0.323}Ga_{0.677}As$(intrinsic) | 600 Å |
| 8 | quantum well | GaAs(intrinsic) | 230 Å |
| 9 | tunnel barrier | $Al_{0.323}Ga_{0.677}As$(intrinsic) | 90 Å |
| 10 | top spacer | GaAs (intrinsic) | 25 Å |
| 11 | top electrode | (n+, $1 \times 10^{18}$) | 200 Å |
| 12 | top electrode | (n+, $4 \times 10^{18}$) | 400 Å |
| 13 | top electrode | Delta doped top layers | 25 Å ×8 |
| | top surface | | |

## 6.1 Mesa Definition and Contact to the Bottom Layer

We cleave the GaAs heterostructure to small pieces(5.5 mm by 5.5 mm) and then we solvent clean with TCE, acetone and IPA. Using photolithography we define the mesa pattern as in Fig 6-1A and isolate the mesa using a wet etch in diluted acid etch: $240 : 8 : 1(H_2O : H_2O_2 : H_2SO_4)$. The etch should remove all the material up to insulating substrate. Hence it is crucial to check the etch depth under a profilemeter. To make contact to the bottom layer, we define pads at both sides of the mesa using photolithography. We deposit a stack of 5 nm Pt, 200 nm Au, 100 nm Ge, 73 nm Pt, 100 nm Au, 50 nm Ge, 55 nm Pt. Annealing this stack to 530°C for 100s, we make a spiky ohmic contact to the bottom layer.

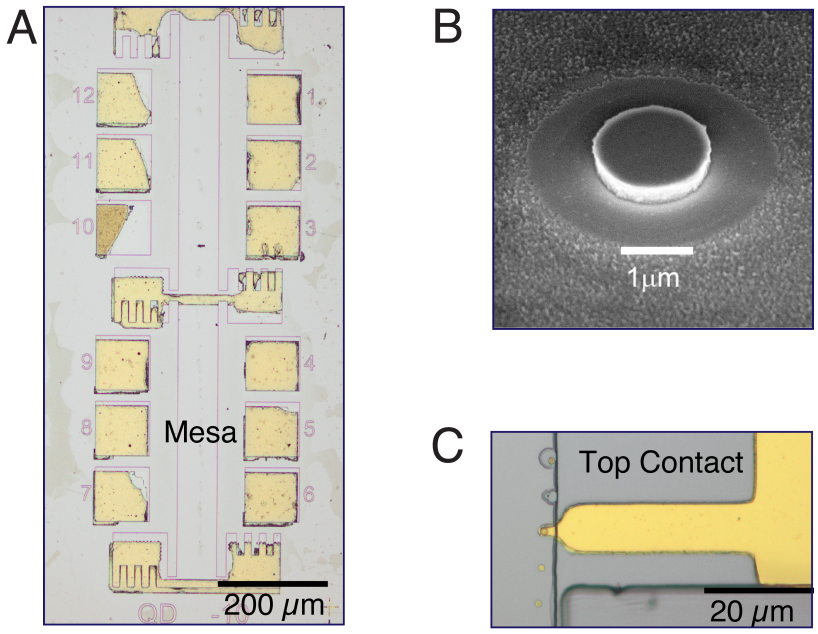


Figure 6-1: (A) Mesa definition and contact to the bottom layer. Here we have three deep ohmic contacts to the bottom electrode, and 12 metallic pads to potentially yield that many devices. (B) An SEM image after the dry etch. (C) A completed device that has contact to a metallic pad.

## 6.2 Ohmic Contacts to the Top Layer

In this step, we define a variety of quantum dots an ebeam writer. To make a low resistance ohmic contact there are various recipes. For our devices we deposit a stack of 60 nm Pd, 170 nm Ge, 10 nm Ti, 50 nm Au. Annealing to 350 °C for 300s, we contact to the top electrode in heterostructure. To isolate the single quantum dots from each other, we utilize the top metal stack as an etch mask. We remove GaAs using $BCl_3\&SF_6$ until it selectively stops at AlGaAs. An SEM image after the dry etch is provided in Fig 6-1B. To connect the pillars to the metallic pads, we perform another e-beam write and deposit a stack of metal. In this last step, we don't need to anneal the stack. A completed device is shown in Fig 6-1C.

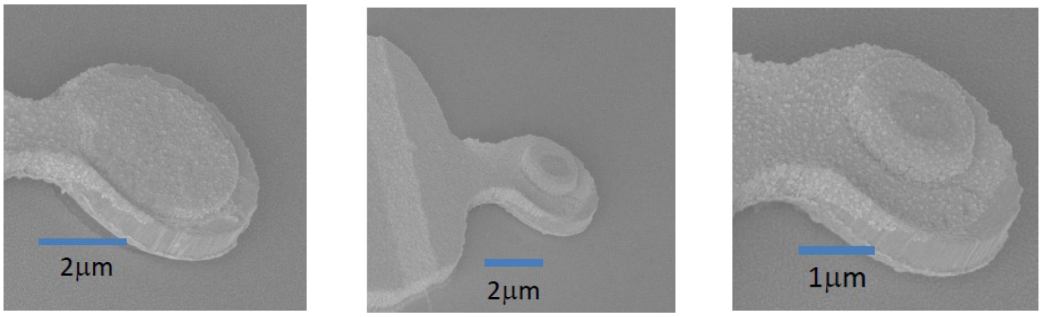


Figure 6-2: The SEM image of the completed devices.

# Chapter 7

# Summary and Directions for Future Research

One of the main advantages of studying vertical quantum dots using single electron capacitance spectroscopy is that it has the capability of probing both localized and delocalized states of electrons. This allows us to study two-dimensional dots of various sizes from small dots to mini 2DEGs. In capacitance experiments, we measure the energies needed to add successive electrons to a quantum dot. Using an electrostatic gate we draw electrons into dot one at a time.

In the small dot regime, we observe distinct electron additions since quantum level spacing and the charging energy is large. The energy spectrum of a small dot under an external magnetic field is well described by Fock-Darwin spectrum. Our experimental data fits well to single particle spectrum with some deviations that arise from electron-electron interaction. Near filling factor $\nu = 1$, we see discontinuities in the single electron additions indicating large tunneling suppression under extreme conditions.

In the medium size dot regime, we can add thousands of electrons into the dot and still resolve single electrons. In high densities, landau levels are formed. In between filled landau levels, we observe localized states where the charge is confined to small puddles. As a result these localized states follow the underlying Landau filling factor.

Our technique allows us to zoom into metallic regions where the landau level is

partially filled. Performing ultra fine measurements at compressible and high density regions, in Figure 5-1 we observe unpredicted states that are evenly spaced in magnetic field. Unlike the electron additions to a small quantum dot where the highest energy electron zig-zags, these periodic states are uniform everywhere. The energies of these states all move down with increasing magnetic field which suggests that they are edge states.

Between filling factor $\nu = 1$ and $\nu = 2$, the periodicity of electron additions correspond to h/e flux addition to the dot where as between filling factor $\nu = 2$ and $\nu = 5$, the periodicity of electron additions is halved. Careful measurements of the peak height showed that between filling factor $\nu = 2$ and $\nu = 5$, a charge 2e is tunneled back and forth to the dat. Contrary to the belief that it would take more energy to add each successive electron to a quantum dot as the electrons would repel each other, our measurements have revealed an astonishing phenomenon: for the high-density regime, electron additions can occur in pairs.

## 7.1 Further Study of Edge States

In this thesis, we have shown various interesting data that show a pairing of two electrons at the edge of a QD. A lot of work is needed to explain the nature of this pairwise attraction. Does the edge turn into a chiral superconductor? What are the relevant energy scales? How can we distinguish this from edge states which are already dissipationless?

To understand the edge states, we need to answer some of these open questions:

- Edge states seem to disappear in between Landau gaps. Why do they disappear?
- We do not see any signature of edge states when the filling factor $\nu = 1$ is partially filled. Is this due to experimental resolution or due to the fact that the edge is not de-coupled from the bulk?
- Why does bunching disappear at filling factor $\nu = 5/2$?

- Above few hundred milliKelvin base temperatures, we observed that the edge states disappear. A careful study is needed to further explain what causes this mechanism.
- We have shown that there are missing bulk states that are invisible to capacitance measurements. Potentially, using smaller dots with higher excitations, we could show possible indications of the bulk states.
- Studying the spin textures of the edge states using parallel magnetic field.

## 7.2 Further Study of Localization

In this thesis we showed data from two different extreme quantum dot sizes. The small dots we measured have an area at the order of $0.02\,\mu m^2$, whereas the medium size dots have area near $0.5\,\mu m^2$. In the medium size dots, the localized states are well defined and lives within incompressible filling factors. Figure 7-1A shows the localized state that is formed in the filling factor $\nu = 1$ and $\nu = 2$. What is surprising to us is that when we follow the kinks in the small dot region, we create these straight lines that is precisely parallel to underlying filling factor. We believe there might be a link between the localized states in the medium size dots and the edge reconstruction in the small dot. The simplest idea is to perform capacitance measurements on a different size dot between these two extremes to unravel the mechanism of localized states.

## 7.3 Spectroscopy of the Excited States in Quantum Dots

Single electron capacitance measurements directly probes only the ground states in the dots. Another very intriguing experiment could be to explore the excited states in the dots, particularly for the edge states we observed. With the time domain spectroscopy[58] we developed in our lab, we can develop a powerful probe for both

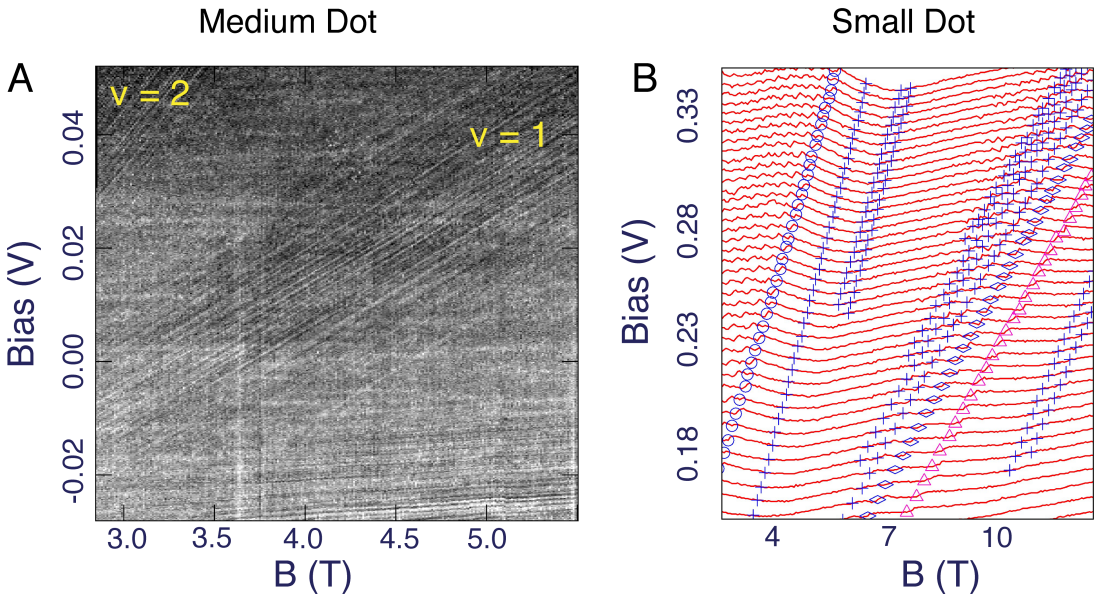


Figure 7-1: Comparison between the localized states in mini 2DEG and the edge reconstruction in very small dots. (A) The localized states within filling factor $\nu = 1$ and $\nu = 2$. When a landau level is fully filled, the fermi energy is within the gap where we can tunnel into charge puddles. (B) In the small dot regime, we observe kinks. Following those kinks, we produce very straight lines that follow the underlying filling factor. Those lines almost look identical to localized states in the medium size dot.

ground states and the excited states. Instead of applying a sinusoidal AC signal, in the time domain spectroscopy we apply a real time pulse to the dot and measure the capacitance response as electrons tunnel from the reservoir to the dot. At the very beginning of the pulse, as electrons tunnel into the dot, they induce an image charge on a nearby gate electrode. Measuring this charge real time, we can deduce the initial tunneling current. The details of how this spectroscopy works is comprehensively explained at Oliver Dial's PhD thesis[59].

If the height of the pulse is just about the charging energy, then one electron is added to the dot. For increasing magnitude of the initial pulse more channels (due to the dot's excited states) will be available for tunneling. By measuring the rate versus the magnitude of the pulse we can map the excitation spectrum of the dot.

In Figure 7-2, we have tried to perform pulsing experiments on a quantum dot. We run the measurements at 4T on a dot that has 3fF capacitance. On the y-axis the excitation pulse goes from -25mV to 25mV. When the dot is depleted(to the left of

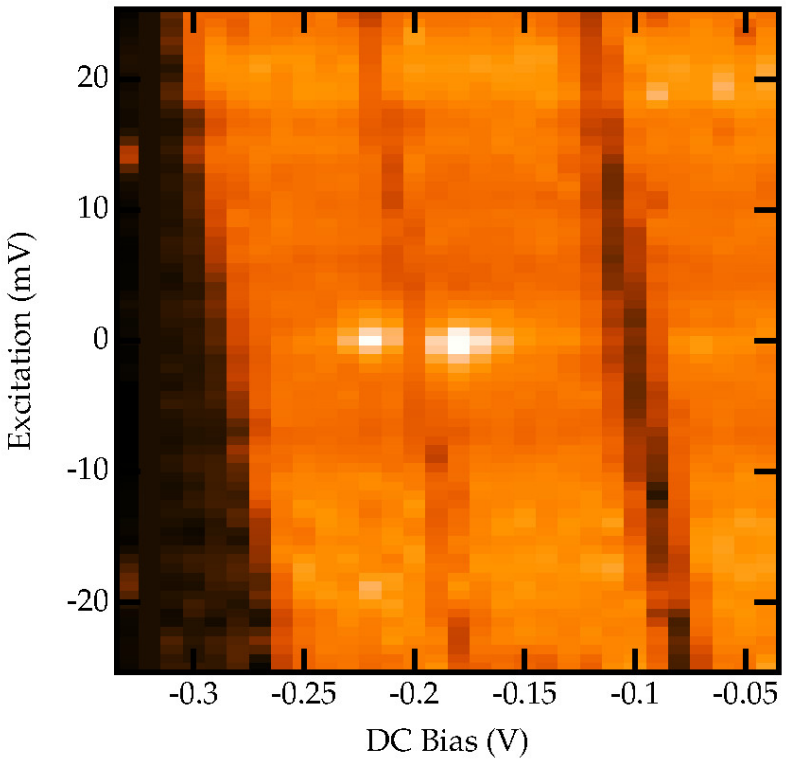


Figure 7-2: The first attempt of a tunneling spectroscopy of a quantum dot. This dot is a relatively large quantum dot that has area of 3fF. The magnetic field is B=4T. We can only see the signatures of formed landau levels.

the Figure 7-2), dark region shows low density of states. And as we gate the sample at B=4T, we can see clear signatures of landau levels despite low signal to noise ratio. In our current structures the barrier is extremely fast. To be able to see excited states we need to lower tunnel barrier in our sample. Since our samples are extremely small, the capacitance change that comes from a single electron is less than 0.01fF. A slower tunnel barrier would allow us to increase averaging time in the charging curve.

THIS PAGE INTENTIONALLY LEFT BLANK

# Appendix A

# Fabrication of GaAs Pillar Quantum Dots

Process for creating sub micron sized pillar shaped quantum dots on high mobility GaAs /AlGaAs heterostructures.

## A.1 Mesa Definition

1. Use 5.5 mm by 5.5 mm GaAs heterostructure
2. Solvent clean wafer
   (a) Sonicate 5min in TCE, Acetone and IPA
3. Spin photoresist (coater in TRL)
   (a) SPR 700 at 4000RPM for 45s for thickness of 1 $\mu$m
   (b) 1 min bake at 95 °C
4. Expose mesa pattern (EV1 in TRL)
   (a) 2.5s exposure
5. Develop (Photo-wet-Au in TRL)

(a) 75s in Dow MF CD-26

6. Etch Mesa (acid-hood in TRL)

   (a) Etch in $240 : 8 : 1(H_2O : H_2O_2 : H_2SO_4)$

   (b) Rate 2.8 nm/s(confirm on a dummy first)

   (c) Etch for 400s($1\mu$m) depending on the wafer.

7. Verify etch depth on dummy wafer (Profilometer)

## A.2 Ohmic Contact to the bottom layer

Process to create the etched gates defining the interferometer.

1. Solvent clean wafer

   (a) Sonicate 5min in TCE, Acetone and IPA

2. Spin photoresist (coater in TRL)

   (a) SPR 700 at 4000RPM for 45s for thickness of 1 $\mu$m

   (b) 1 min bake at 95 °C

3. Expose mesa pattern (EV1 in TRL)

   (a) 2.5s exposure

4. Develop (Photo-wet-Au in TRL)

   (a) 75s in Dow MF CD-26

5. Short oxide etch (Acid hood in TRL)

   (a) $10 : 1$ $H_2 : HCl$ for $5s$

6. E-beam evaporate Ohmic metal Stack(EbeamAu in TRL)

(a) Deposit a stack of 5 nm Pt, 200 nm Au, 100 nm Ge, 73 nm Pt, 100 nm Au, 50 nm Ge, 55 nm Pt

7. Liftoff using Acetone (Photo-wet-Au in TRL)

   (a) Rinse in IPA, (water afterwards only in TRL).

8. Anneal the ohmics. (RTA in TRL)

   (a) Anneal to 530 °C for 100s

## A.3 Pillar definition/Ohmic Contacts to the top

Process for defining the pillars using an AlGaAs etch stop, and utilizing the ohmic contacts as a self- aligned etch mask.

1. Solvent clean wafer

   (a) Sonicate 5min in TCE, Acetone and IPA

2. Spin PMMA (PMMA spinner)

   (a) 4000RPM A11 45s, bake 180 °C for 3 min

   (b) 4000RPM A4 45s, bake 180 °C for 3 min

3. Expose PMMA using ebeam writer (Raith)

   (a) 10KeV, 30$\mu$m Aperture, 275$\mu C/cm^2$ Dose, 26nm Grid size

4. Develop (Photo-wet-Au in TRL)

   (a) MIBK:IPA (1 : 3) for 60s and IPA for 15s

5. Short oxide etch (Acid hood in TRL)

   (a) 10 : 1 $H_2 : HCl$ for 5s

6. E-beam evaporate Ohmic metal Stack(EbeamAu in TRL)

(a) Deposit a stack of 60 nm Pd, 170 nm Ge, 10 nm Ti, 50 nm Au

7. Liftoff using Acetone (Photo-wet-Au in TRL)

   (a) Rinse in IPA and water afterwards

8. Anneal the ohmics. (RTA in TRL)

   (a) Anneal to 350 °C for 300s

9. Etch Pillar using $BCl_3$&$SF_6$ with low bias voltage 80V to selectively etch GaAs and stop at AlGaAs (Plasmaquest in TRL)

   (a) $BCl_3 = 51$sccm, $SF_6 = 17$sccm, Pressure=37.5mTorr, Bias=80V

   (b) Etch rate at GaAs is roughly 5 $A°/s$

10. Verify pillar quality using SEM. (Optional)

## A.4 Contact to the top ohmic

Process to create the top gates defining the interferometer and plungers.

1. Solvent clean wafer

   (a) Sonicate 5min in TCE, Acetone and IPA

2. Spin photoresist (coater in TRL)

   (a) SPR 700 at 4000RPM for 45s for thickness of $1\mu m$

   (b) 1 min bake at 95 °C

3. Expose mesa pattern (EV1 in TRL)

   (a) 2.5s exposure

4. Develop (Photo-wet-Au in TRL)

   (a) 75s in Dow MF CD-26

5. Etch up to insulating layer to disconnect top and bottom ohmics(Acid hood in TRL)
    (a) Etch in $240 : 8 : 1 (H_2O : H_2O_2 : H_2SO_4)$
    (b) Rate  2.8 nm/s
    (c) Etch for 280s(700nm)
6. Spin PMMA (PMMA spinner)
    (a) 4000RPM A11 45s, bake 180 °C for 3 min
    (b) 4000RPM A11 45s, bake 180 °C for 3 min
    (c) 4000RPM A4 45s, bake 180 °C for 3 min
7. $10nm$ Au deposition (EbeamFP in TRL)
8. Expose PMMA using ebeam writer (Raith)
    (a) 10KeV, 120$\mu$m Aperture, 275$\mu C/cm^2$ Dose, 26nm Grid size
9. Develop (Photo-wet-Au in TRL)
    (a) MIBK:IPA $(1 : 3)$ for 60s and IPA for 15s
10. E-beam evaporate Ohmic metal Stack(EbeamAu in TRL)
    (a) Deposit a stack of Ti/Au/Ag/Au (Thick enough to exceed the etch, roughly 800nm)
11. Liftoff using Acetone (Photo-wet-Au in TRL)
    (a) Rinse in IPA and water afterwards
12. Don't anneal the last metal stack.

THIS PAGE INTENTIONALLY LEFT BLANK

# Appendix B

# The List of Fabricated Quantum Dots

Based on the capacitance data, we estimate that the dot diameter is 0.6 mm less than lithographic diameter due to undercut. We have taken the small dot capacitance data from QD 1-5. The edge states has been observed at QD 5-6 and 5-2.

| Mesa | Device | Lith d($\mu m$) | Contacted | Mesa | Device | Lith d($\mu m$) | Contacted |
|---|---|---|---|---|---|---|---|
| 1 | 1 | 0.4 | Yes | 2 | 1 | 1 | Yes |
| 1 | 12 | 0.45 | Yes | 2 | 12 | 1.05 | Yes |
| 1 | 2 | 0.5 | Yes | 2 | 2 | 1.1 | Yes |
| 1 | 11 | 0.55 | Maybe | 2 | 11 | 1.15 | Yes |
| 1 | 3 | 0.6 | Yes | 2 | 3 | 1.2 | Yes |
| 1 | 10 | 0.65 | Yes | 2 | 10 | 1.25 | Yes |
| 1 | 4 | 0.7 | Yes | 2 | 4 | 1.3 | Yes |
| 1 | 9 | 0.75 | Yes | 2 | 9 | 1.35 | Yes |
| 1 | 5 | 0.8 | Yes | 2 | 5 | 1.4 | Yes |
| 1 | 8 | 0.85 | Maybe | 2 | 8 | 1.45 | Yes |
| 1 | 6 | 0.9 | Yes | 2 | 6 | 1.5 | Yes |
| 1 | 7 | 0.95 | Yes | 2 | 7 | 1.55 | Yes |

| Mesa | Device | Lith d($\mu m$) | Contacted | Mesa | Device | Lith d($\mu m$) | Contacted |
|---|---|---|---|---|---|---|---|
| 3 | 1 | 1.6 | Yes | 4 | 1 | 0.4 | Yes |
| 3 | 12 | 1.7 | Yes | 4 | 12 | 0.45 | Yes |
| 3 | 2 | 2 | Yes | 4 | 2 | 0.5 | Yes |
| 3 | 11 | 3 | Yes | 4 | 11 | 0.55 | Maybe |
| 3 | 3 | 4 | No | 4 | 3 | 0.6 | Maybe |
| 3 | 10 | 6 | Yes | 4 | 10 | 0.65 | Maybe |
| 3 | 4 | 1.6 | No | 4 | 4 | 0.7 | Yes |
| 3 | 9 | 1.7 | Yes | 4 | 9 | 0.75 | Yes |
| 3 | 5 | 2 | Yes | 4 | 5 | 0.8 | Maybe |
| 3 | 8 | 3 | Yes | 4 | 8 | 0.85 | Yes |
| 3 | 6 | 4 | No | 4 | 6 | 0.9 | Yes |
| 3 | 7 | 6 | Yes | 4 | 7 | 0.95 | Yes |
| 5 | 1 | 1 | No | 6 | 1 | 0.4 | Maybe |
| 5 | 12 | 1.05 | Yes | 6 | 12 | 0.45 | Maybe |
| 5 | 2 | 1.1 | Yes | 6 | 2 | 0.5 | Yes |
| 5 | 11 | 1.15 | Yes | 6 | 11 | 0.55 | Maybe |
| 5 | 3 | 1.2 | Yes | 6 | 3 | 0.6 | Yes |
| 5 | 10 | 1.25 | Yes | 6 | 10 | 0.65 | Yes |
| 5 | 4 | 1.3 | Yes | 6 | 4 | 0.7 | Yes |
| 5 | 9 | 1.35 | Yes | 6 | 9 | 0.75 | Maybe |
| 5 | 5 | 1.4 | Yes | 6 | 5 | 0.8 | Yes |
| 5 | 8 | 1.45 | Yes | 6 | 8 | 0.85 | Yes |
| 5 | 6 | 1.5 | Yes | 6 | 6 | 0.9 | Yes |
| 5 | 7 | 1.55 | Yes | 6 | 7 | 0.95 | Yes |

| Mesa | Device | Lith d($\mu m$) | Contacted | Mesa | Device | Lith d($\mu m$) | Contacted |
|---|---|---|---|---|---|---|---|
| 7 | 1 | 1 | Maybe | 8 | 1 | 1.6 | Yes |
| 7 | 12 | 1.05 | Yes | 8 | 12 | 1.7 | Yes |
| 7 | 2 | 1.1 | Yes | 8 | 2 | 2 | Yes |
| 7 | 11 | 1.15 | Yes | 8 | 11 | 3 | Yes |
| 7 | 3 | 1.2 | Yes | 8 | 3 | 4 | Yes |
| 7 | 10 | 1.25 | Yes | 8 | 10 | 6 | Yes |
| 7 | 4 | 1.3 | Yes | 8 | 4 | 1.6 | Yes |
| 7 | 9 | 1.35 | Yes | 8 | 9 | 1.7 | Yes |
| 7 | 5 | 1.4 | Yes | 8 | 5 | 2 | Yes |
| 7 | 8 | 1.45 | Yes | 8 | 8 | 3 | Yes |
| 7 | 6 | 1.5 | Yes | 8 | 6 | 4 | No |
| 7 | 7 | 1.55 | Yes | 8 | 7 | 6 | Yes |
| 9 | 1 | 0.4 | Maybe | 10 | 1 | 1 | No |
| 9 | 12 | 0.45 | No | 10 | 12 | 1.05 | Maybe |
| 9 | 2 | 0.5 | Maybe | 10 | 2 | 1.1 | Yes |
| 9 | 11 | 0.55 | No | 10 | 11 | 1.15 | Yes |
| 9 | 3 | 0.6 | Maybe | 10 | 3 | 1.2 | No |
| 9 | 10 | 0.65 | No | 10 | 10 | 1.25 | Maybe |
| 9 | 4 | 0.7 | Yes | 10 | 4 | 1.3 | No |
| 9 | 9 | 0.75 | No | 10 | 9 | 1.35 | Yes |
| 9 | 5 | 0.8 | Yes | 10 | 5 | 1.4 | No |
| 9 | 8 | 0.85 | Maybe | 10 | 8 | 1.45 | Yes |
| 9 | 6 | 0.9 | Yes | 10 | 6 | 1.5 | No |
| 9 | 7 | 0.95 | Yes | 10 | 7 | 1.55 | Yes |

# Bibliography


[1] H.K. Choi, I. Sivan, A. Rosenblatt, M. Heiblum, V. Umansky, and D. Mahalu. Robust electron pairing in the integer quantum hall effect regime. *Nature Communications*, 6(1), December 2015.

[2] K. v. Klitzing, G. Dorda, and M. Pepper. New Method for High-Accuracy Determination of the Fine-Structure Constant Based on Quantized Hall Resistance. *Physical Review Letters*, 45(6):494–497, August 1980.

[3] D. C. Tsui, H. L. Stormer, and A. C. Gossard. Two-Dimensional Magnetotransport in the Extreme Quantum Limit. *Physical Review Letters*, 48(22):1559–1562, May 1982.

[4] J. K. Jain. Composite-fermion approach for the fractional quantum Hall effect. *Physical Review Letters*, 63(2):199–202, July 1989.

[5] Gregory Moore and Nicholas Read. Nonabelions in the fractional quantum hall effect. *Nuclear Physics B*, 360(2-3):362–396, August 1991.

[6] Martin Greiter, Xiao-Gang Wen, and Frank Wilczek. Paired Hall state at half filling. *Physical Review Letters*, 66(24):3205–3208, June 1991.

[7] J. P. Eisenstein and H. L. Stormer. The Fractional Quantum Hall Effect. *Science*, 248(4962):1510–1516, June 1990.

[8] V. S. Khrapai, A. A. Shashkin, M. G. Trokina, V. T. Dolgopolov, V. Pellegrini, F. Beltram, G. Biasiol, and L. Sorba. Direct Measurements of Fractional Quantum Hall Effect Gaps. *Physical Review Letters*, 99(8), August 2007.

[9] V. S. Khrapai, A. A. Shashkin, M. G. Trokina, V. T. Dolgopolov, V. Pellegrini, F. Beltram, G. Biasiol, and L. Sorba. Filling Factor Dependence of the Fractional Quantum Hall Effect Gap. *Physical Review Letters*, 100(19), May 2008.

[10] D. G. Polyakov and B. I. Shklovskii. Activated Conductivity in the Quantum Hall Effect. *Physical Review Letters*, 73(8):1150–1153, August 1994.

[11] F. Hohls, U. Zeitler, and R. J. Haug. Hopping Conductivity in the Quantum Hall Effect: Revival of Universal Scaling. *Physical Review Letters*, 88(3), January 2002.

[12] M. M. Fogler, A. A. Koulakov, and B. I. Shklovskii. Ground state of a two-dimensional electron liquid in a weak magnetic field. *Physical Review B*, 54(3):1853–1871, July 1996.

[13] R. L. Willett, L. N. Pfeiffer, and K. W. West. Alternation and interchange of e/4 and e/2 period interference oscillations consistent with filling factor 5/2 non-Abelian quasiparticles. *Physical Review B*, 82(20), November 2010.

[14] A. Y. Cho. Growth of Periodic Structures by the Molecular-Beam Method. *Applied Physics Letters*, 19(11):467–468, December 1971.

[15] Leo Kouwenhoven and Charles Marcus. Quantum dots. *Physics World*, 11(6):35–40, June 1998.

[16] Marc A. Kastner. Artificial Atoms. *Physics Today*, 46(1):24–31, January 1993.

[17] S. Tarucha, D. G. Austing, T. Honda, R. J. van der Hage, and L. P. Kouwenhoven. Shell Filling and Spin Effects in a Few Electron Quantum Dot. *Physical Review Letters*, 77(17):3613–3616, October 1996.

[18] T. H. Oosterkamp, J. W. Janssen, L. P. Kouwenhoven, D. G. Austing, T. Honda, and S. Tarucha. Maximum-Density Droplet and Charge Redistributions in Quantum Dots at High Magnetic Fields. *Physical Review Letters*, 82(14):2931–2934, April 1999.

[19] N. B. Zhitenev. Localization-Delocalization Transition in Quantum Dots. *Science*, 285(5428):715–718, July 1999.

[20] R. C. Ashoori. Electrons in artificial atoms. *Nature*, 379(6564):413–419, February 1996.

[21] R. C. Ashoori, H. L. Stormer, J. S. Weiner, L. N. Pfeiffer, K. W. Baldwin, and K. W. West. N-electron ground state energies of a quantum dot in magnetic field. *Physical Review Letters*, 71(4):613–616, July 1993.

[22] R. C. Ashoori, H. L. Stormer, J. S. Weiner, L. N. Pfeiffer, S. J. Pearton, K. W. Baldwin, and K. W. West. Single-electron capacitance spectroscopy of discrete quantum levels. *Physical Review Letters*, 68(20):3088–3091, May 1992.

[23] Lydia L. Sohn, Leo P. Kouwenhoven, and Gerd Schön, editors. *Mesoscopic Electron Transport*. Springer Netherlands, Dordrecht, 1997.

[24] Hermann Grabert and Michel H. Devoret, editors. *Single Charge Tunneling*, volume 294 of *NATO ASI Series*. Springer US, Boston, MA, 1992.

[25] L.I.Glazman and K.A. Matveev. Removal of coulomb blockade of one-electron tunneling by quantum fluctuation. *Sov. Phys. JETP*, 71:1031, 1990.

[26] K.A. Matveev. Quantum fluctuation of metallic particle charge under coulomb blockade conditions. *Sov. Phys. JETP*, 72:892, 1991.

[27] R.C. Ashoori, H.L. Stormer, J.S. Weiner, L.N. Pfeiffer, S.J. Pearton, K.W. Baldwin, and K.W. West. Single-electron capacitance spectroscopy of a few electron box. *Physica B: Condensed Matter*, 189(1-4):117–124, June 1993.

[28] R. Dingle, H. L. Störmer, A. C. Gossard, and W. Wiegmann. Electron mobilities in modulation-doped semiconductor heterojunction superlattices. *Applied Physics Letters*, 33(7):665–667, October 1978.

[29] S. Weinreb, J. Bardin, H. Mani, and G. Jones. Matched wideband low-noise amplifiers for radio astronomy. *Review of Scientific Instruments*, 80(4):044702, April 2009.

[30] R. C. Ashoori, J. A. Lebens, N. P. Bigelow, and R. H. Silsbee. Equilibrium tunneling from the two-dimensional electron gas in GaAs: Evidence for a magnetic-field-induced energy gap. *Physical Review Letters*, 64(6):681–684, February 1990.

[31] R. H. Silsbee and R. C. Ashoori. Comment on "Zeeman bifurcation of quantum-dot spectra". *Physical Review Letters*, 64(16):1991–1991, April 1990.

[32] C. W. J. Beenakker. Theory of Coulomb-blockade oscillations in the conductance of a quantum dot. *Physical Review B*, 44(4):1646–1656, July 1991.

[33] V. Fock. Bemerkung zur Quantelung des harmonischen Oszillators im Magnetfeld. *Zeitschrift fur Physik*, 47(5-6):446–448, May 1928.

[34] C. G. Darwin. The Diamagnetism of the Free Electron. *Mathematical Proceedings of the Cambridge Philosophical Society*, 27(01):86, January 1931.

[35] Arvind Kumar, Steven E. Laux, and Frank Stern. Electron states in a GaAs quantum dot in a magnetic field. *Physical Review B*, 42(8):5166–5175, September 1990.

[36] Ah MacDonald, Sr Eric Yang, and Md Johnson. Quantum Dots in Strong Magnetic Fields: Stability Criteria for the Maximum Density Droplet. *Australian Journal of Physics*, 46(3):345, 1993.

[37] Jainendra Jain. *Composite Fermions*. Cambridge University Press, Cambridge, 2007.

[38] R. Willett, J. P. Eisenstein, H. L. Störmer, D. C. Tsui, A. C. Gossard, and J. H. English. Observation of an even-denominator quantum number in the fractional quantum Hall effect. *Physical Review Letters*, 59(15):1776–1779, October 1987.

[39] Sankar Das Sarma, Michael Freedman, and Chetan Nayak. Topologically Protected Qubits from a Possible Non-Abelian Fractional Quantum Hall State. *Physical Review Letters*, 94(16), April 2005.

[40] A.Yu. Kitaev. Fault-tolerant quantum computation by anyons. *Annals of Physics*, 303(1):2–30, January 2003.

[41] Chetan Nayak, Steven H. Simon, Ady Stern, Michael Freedman, and Sankar Das Sarma. Non-Abelian anyons and topological quantum computation. *Reviews of Modern Physics*, 80(3):1083–1159, September 2008.

[42] A.L. Efros. Non-linear screening and the background density of 2DEG states in magnetic field. *Solid State Communications*, 67(11):1019–1022, September 1988.

[43] D. B. Chklovskii, B. I. Shklovskii, and L. I. Glazman. Electrostatics of edge channels. *Physical Review B*, 46(7):4026–4034, August 1992.

[44] S. Ilani, J. Martin, E. Teitelbaum, J. H. Smet, D. Mahalu, V. Umansky, and A. Yacoby. The microscopic nature of localization in the quantum Hall effect. *Nature*, 427(6972):328–332, January 2004.

[45] Dmitri B. Chklovskii and Patrick A. Lee. Transport properties between quantum Hall plateaus. *Surface Science*, 305(1-3):133–138, March 1994.

[46] N. R. Cooper and J. T. Chalker. Coulomb interactions and the integer quantum Hall effect: Screening and transport. *Physical Review B*, 48(7):4530–4544, August 1993.

[47] M. J. Yoo. Scanning Single-Electron Transistor Microscopy: Imaging Individual Charges. *Science*, 276(5312):579–582, April 1997.

[48] N. B. Zhitenev, T. A. Fulton, A. Yacoby, H. F. Hess, L. N. Pfeiffer, and K. W. West. Imaging of localized electronic states in the quantum Hall regime. *Nature*, 404(6777):473–476, March 2000.

[49] Ah MacDonald, Sr Eric Yang, and Md Johnson. Quantum Dots in Strong Magnetic Fields: Stability Criteria for the Maximum Density Droplet. *Australian Journal of Physics*, 46(3):345, 1993.

[50] C. de C. Chamon and X. G. Wen. Sharp and smooth boundaries of quantum Hall liquids. *Physical Review B*, 49(12):8227–8241, March 1994.

[51] R. C. Ashoori, J. A. Lebens, N. P. Bigelow, and R. H. Silsbee. Energy gaps of the two-dimensional electron gas explored with equilibrium tunneling spectroscopy. *Physical Review B*, 48(7):4616–4628, August 1993.

[52] A. M. Chang. Chiral Luttinger liquids at the fractional quantum Hall edge. *Reviews of Modern Physics*, 75(4):1449–1505, November 2003.

[53] M. M. Fogler, E. I. Levin, and B. I. Shklovskii. Chemical potential and magnetization of a Coulomb island. *Physical Review B*, 49(19):13767–13775, May 1994.

[54] I. Sivan, R. Bhattacharyya, H. K. Choi, M. Heiblum, D. E. Feldman, D. Mahalu, and V. Umansky. Interaction-induced interference in the integer quantum Hall effect. *Physical Review B*, 97(12), March 2018.

[55] Bertrand I. Halperin, Ady Stern, Izhar Neder, and Bernd Rosenow. Theory of the Fabry-Pérot quantum Hall interferometer. *Physical Review B*, 83(15), April 2011.

[56] J. M. Luttinger. An Exactly Soluble Model of a Many-Fermion System. *Journal of Mathematical Physics*, 4(9):1154–1162, September 1963.

[57] F D M Haldane. 'Luttinger liquid theory' of one-dimensional quantum fluids. I. Properties of the Luttinger model and their extension to the general 1D interacting spinless Fermi gas. *Journal of Physics C: Solid State Physics*, 14(19):2585–2609, July 1981.

[58] Ho Bun Chan. *Tunneling Spectroscopy of the Two-Dimensional Electron Gas*. PhD thesis, Massachusetts Institute of Technology, 1999.

[59] Oliver Eugene Dial. *Single Particle Spectrum of the Two Dimensional Electron Gas*. PhD thesis, Massachusetts Institute of Technology, 2007.